United States Department of Commerce
Technology Administration
National Institute of Standards and Technology

NISTIR 5038

Report No. 28
RESIDUAL STRESS IN INDUCTION-HEATED RAILROAD WHEELS: ULTRASONIC AND SAW CUT MEASUREMENTS

Raymond E. Schramm
Jacek Szelążek
Alfred V. Clark, Jr.

NISTIR 5038

Report No. 28
RESIDUAL STRESS IN INDUCTION-HEATED RAILROAD WHEELS: ULTRASONIC AND SAW CUT MEASUREMENTS

Raymond E. Schramm
Jacek Szelążek
Alfred V. Clark, Jr.

Materials Reliability Division
Material Science and Engineering Laboratory
National Institute of Standards and Technology
Boulder, Colorado 80303

Prepared for
U.S. Department of Transportation
Federal Railroad Administration
Office of Research and Development
Washington, D.C. 20590

May 1995

U.S. DEPARTMENT OF COMMERCE, Ronald H. Brown, Secretary
TECHNOLOGY ADMINISTRATION, Mary L. Good, Under Secretary for Technology
NATIONAL INSTITUTE OF STANDARDS AND TECHNOLOGY, Arati Prabhakar, Director

CONTENTS

LIST OF SYMBOLS

Abbreviations

brf - Back Rim Face
D - Flange Tip Opening Displacement
DE - Destructive Evaluation
EMAT - Electromagnetic-Acoustic Transducer
FRA - Federal Railroad Administration
frf - Front Rim Face
NDE - Nondestructive Evaluation
NIST - National Institute of Standards and Technology
PET - Piezoelectric Transducer
SSW - Surface-Skimming Wave
TOF - Time of Flight
TTC - Transportation Technology Center, Association of American Railroads

Symbols

B - Total Birefringence
B_0 - Birefringence Due to Texture
C_A - Stress Acoustic Constant for Shear Waves Traveling Normal to Stress
C_F - Stress Acoustic Constant for Surface Waves
C_S - Stress Acoustic Constant for Longitudinal Waves Traveling Along Stress
e - Elastic State
F_N - Net Rim Force
L - Longitudinal Wave
N - Number of Specimens
r - Radial Direction, or Reference
s - Stressed State
S - Shear Wave
SD - Standard Deviation
t - Time
T - Temperature
V - Velocity
α - Integration Constant
β - Integration Constant
Δ - Change, Difference
θ - Hoop Direction
ρ - Mass Density
σ - Stress

Units

hp - Horsepower
ksi - 1000 Pounds per Square Inch
kW - kilowatt
MHz - 10^6 Hertz
mm - 10^{-3} Meter
MPa - 10^6 Pascals
μm - 10^{-6} Meter

Residual Stress in Induction-Heated Railroad Wheels: Ultrasonic and Saw Cut Measurements

Raymond E. Schramm, Jacek Szelążek,* and Alfred V. Clark, Jr.

Materials Reliability Division
Materials Science and Engineering Laboratory
National Institute of Standards and Technology
Boulder, Colorado 80303-3328

This is Report Number 28 in a series covering research performed by the National Institute of Standards and Technology for the Federal Railroad Administration. This report covers a project by the Materials Reliability Division to develop and test an ultrasonic system to measure residual stress in the rims of railroad wheels.

This nondestructive evaluation uses the acoustoelastic effect, a small change of sound wave velocity due to the effect of stress on elastic parameters. To make more than one thousand stress measurements, we used two types of ultrasonic transducers, piezoelectric and electromagnetic, to probe both thickness-averaged and near-surface stresses in the rim of railroad wheels. The test specimens were unused, cast-steel wheels from the same production run. Eight of our ten wheels had received three levels of induction heating at the tread to simulate the effects of drag-braking that can generate tensile hoop stress. After the nondestructive tests, three wheels were cut with a saw along a radius to measure flange tip opening and verify the stress state. The displacement of the opening (after cutting completely through the rim) is proportional to the net rim force. We found good correlation between a subset of ultrasonic measurements and the saw cut opening, and this indicates that this approach may be useful for field assessment of wheel safety. Wheels with negative net rim force are in compression and will likely arrest any cracks. Wheels with positive rim force are likely to suffer failure by crack propagation.

Key words: EMAT; nondestructive testing; piezoelectric; railroad wheel; residual stress; ultrasonic

* NIST Guest Researcher on leave from the Institute of Fundamental Technological Research, Polish Academy of Sciences, Warsaw

1. CONTRACT HISTORY

Our work to develop ultrasonic nondestructive evaluation methods for railroad wheels began in 1985. While the original emphasis was on roll-by detection of tread cracks, the emphasis has changed to include the measurement of hoop residual stress in the rims. Here, the goal is to develop a reliable, quantitative method that is useful in a wheel shop environment. This work was done under a three-year research contract, Reimbursable Agreement No. DTFR53-91-X-0068 with an effective date of May 30, 1991.

We have made oral presentations of parts of this work at several technical meetings:

1. "Status of EMAT Development for Inspection of Railroad Wheels at NIST," *Seminar on Wheel Thermal Damage Mechanisms*, Central Institute of the Polish State Railways (CNTK), Warsaw, May 19-20, 1993.

2. "Ultrasonic Measurement of Residual Stress in Railroad Wheels," *Spring Conference, American Society for Nondestructive Testing*, March 21-25, 1994, New Orleans.

3. "Residual Stress in Induction Heated Railroad Wheels: Comparison of Ultrasonic and Sawcut Measurements," *Fourth International Conference on Residual Stresses*, Baltimore, June 8-10, 1994.

Other presentations that resulted in formal publications are:

1. R.E. Schramm, A.V. Clark, and T.J. McGuire, "Ultrasonic Measurement of Residual Stress in Railroad Wheel Rims," *Proceedings, Tenth International Wheelset Congress*, National Conference Publication (The Institution of Engineers, Australia, Sydney, 1992), pp. 151-155.

2. R.E. Schramm, A.V. Clark, and J. Szelążek, "Ultrasonic Measurement of Residual Stress in Cast Steel Railroad Wheels,"*Proceedings, The 1994 Pressure Vessels and Piping Conference*, Minneapolis, Minnesota, ed. J. C. Spanner, Jr., PVP-Vol. 276, NDE-Vol. 12 (ASME, NY, 1994), pp. 157-162.

2. INTRODUCTION

The replacement of railroad wheels in the United States is big business. A 1985 article estimated the cost to be about $500 million annually [1]. Most of this is due to simple wear and tear indicating the end of normal operating life and requiring retirement from service. However, a significant subset of these costs is due to the condemnation of wheels suspected of receiving thermal abuse from severe drag-braking.

As-manufactured, cast wheel rims contain compressive residual hoop stress. High power drag-braking will heat the rim and may reverse this stress, a condition that can contribute to crack growth and possible failure. While the number of derailments directly traceable to such failures is relatively small, the consequences are considerable. Enforcement is currently suspended, but a Federal Railroad Administration (FRA) regulation requires removal of wheels when a heating discoloration extends 100 mm (4 in) or more into the plate area [2]. Such a colored band is due to oxides resulting from heat that can be a necessary, but not sufficient, condition for tensile residual stresses to build up in the rim area. However, it is possible to have discoloration with low heat applied for a long time while the wheel retains its original, safe condition. Approximately 180,000 suspect wheels are replaced annually under this rule at $1,000 each [1]. Studies have shown that about half are still in rim compression [3-5]; this means an estimated loss of $90 million each year due to unnecessary wheel removal [1,4].

A nondestructive method to measure residual stress quantitatively could have a substantial impact on reducing these costs and yet contribute to safer operations. Such methods as X-rays or Barkhausen noise measure only near-surface stress. Bulk stresses are more likely to be significant for safety. Ultrasonics may be a practical means to probe these stresses that cause small but measurable changes in the velocity of sound waves [6]. However, since this effect is small, other influences (for example variations in material texture) are significant [6,7]. There are two potentially useful nondestructive evaluation (NDE) methods: (1) Orthogonally polarized shear waves propagate through the specimen and the difference in their velocities (birefringence) gives thickness-averaged stress. (2) Waves propagate along the top few millimeters of the surface; any velocity changes, compared to an unstressed (reference) sample, indicate near-surface stresses. More theory supporting these techniques is below.

In the first (1984) ultrasonic measurements of hoop residual stress in the rims of monoblock railroad wheels [8], some specimens were rolled and some cast. Measurements on rolled wheels agree with results of destructive evaluation (DE) to within 40 MPa. Birefringence measurements in 1986 on in-service, cast-steel wheels used both electromagnetic-acoustic transducers (EMATs) and piezoelectric transducers (PETs) [9]. Results from these two transducers were in good agreement.

In 1987, stress development in forged wheels was the subject of both ultrasonic and X-ray diffraction tests on forged wheels in Vitry, France [10]. Several wheels received several dynamometer brakings. Each cycle lasted 45 min at four braking powers ranging from 20 to 50 kW. Tests included both surface skimming waves (SSWs) and the birefringence technique. There was good agreement among the methods. In 1988, the first field measurements on forged wheels occurred in Velim, Czech Republic [11]. The brake power to four wheels rolling on a track was 20 to 50 kW. The same two ultrasonic methods showed axisymetric stress distributions in the wheel rims.

Additional PET measurements were made in 1988 on cast wheels [12]. Several used wheels received additional inductive heating of 17 kW and 22 kW for 60 min. Pressure and shear waves propagating near the surface probed the rim on the back face. In the 22-kW wheels, the tensile stress was 120-170 MPa; at 17 kW, the tensile stress was lower at 85 to 120 MPa. Relatively high differences between the wheels subjected to the same inductive heat loads are probably the result of unknown residual stresses created during service. These tests included three new wheels where the residual hoop stresses on the back face surfaces ranged from 40 to 100 MPa in compression. All the ultrasonic measurements correlated with saw cutting. Still other measurements on cast wheels with the same apparatus [13] showed saw cut opening or closing related to tension or compression in the rims.

This report deals principally with the ultrasonic measurement of residual stress in a set of 10 cast steel wheels of U.S. manufacture. They were all from the same heat, and so had the same chemical composition. Two wheels remained as manufactured with hoop compression in the rim. The others received three levels of induction heating at the tread to reverse the stress (give tensile stress in the rim). This form of heat damage should generate an idealized, axisymmetric stress state, in contrast to drag braking, where local high spots on the tread can lead to hot spots and stresses that vary around the circumference. Experimentally, an axisymmetric stress helps to reduce the number of ultrasonic measurements. It also greatly simplifies the labor (both experimental and computational) necessary to perform DE for an independent validation of the ultrasonic measurements.

The ultrasonic measurements employed two different types of transducers. Conventional PETs were used for both birefringence and surface stress measurements. These were part of a portable stress instrument (DEBRO*) developed by the Institute of Fundamental Technological Research of the Polish Academy of Sciences. This is the instrument used in the experiments described in Refs. [9-12]. An acoustic couplant was necessary to transfer the signal between

* The use of tradenames is included only for identification and neither constitutes nor implies endorsement or approval by NIST.

transducer and specimen. The fixtures for the transducers had permanent magnets to hold onto the wheels.

EMATs use a coil close to the surface of the specimen to generate a high-frequency eddy current. This interacts with an externally imposed magnetic induction to produce a force on the atomic lattice that sets up ultrasonic waves [14]. Since the signal exists only within the specimen, no couplant is necessary and scanning is easy. The EMATs used here were of our own design [15,16] and generated orthogonally polarized shear waves traveling along a surface normal. In a nonmagnetic material, EMATs generate ultrasonic waves solely by the reaction force (Lorentz force) between eddy currents and magnetic induction. However, other transduction mechanisms also occur in magnetic materials (such as cast wheels) [14,17]. Waves generated by magnetostriction are out of phase with those from the Lorentz force [18]; interference between the two waves can cause artifacts in time-of-flight (TOF) measurements. Therefore, one of our research goals is to compare EMAT and PET results since there is no such interference in the latter.

Following our extensive NDE measurements, the manufacturer made radial saw cuts on three heated wheels. The degree and direction of the opening displacement indicate the forces in the rim. As in prior work cited above, this was necessary to validate the ultrasonic methods.

3. ULTRASONIC THEORY

3.1 Acoustic Birefringence for Thickness-Averaged Stress

A body of acoustic theory has developed [7]. In summary, birefringence B is the velocity difference between two orthogonally polarized shear waves. The (normalized) difference is

$$B = 2\frac{(V_\theta - V_r)}{(V_\theta + V_r)}, \tag{1}$$

where V_θ and V_r are velocities of waves polarized in the hoop and radial directions (Fig. 1a). To find B, we measure the TOFs because the path length is the same for both waves. Then

$$B = 2\frac{(t_r - t_\theta)}{(t_\theta + t_r)}. \tag{2}$$

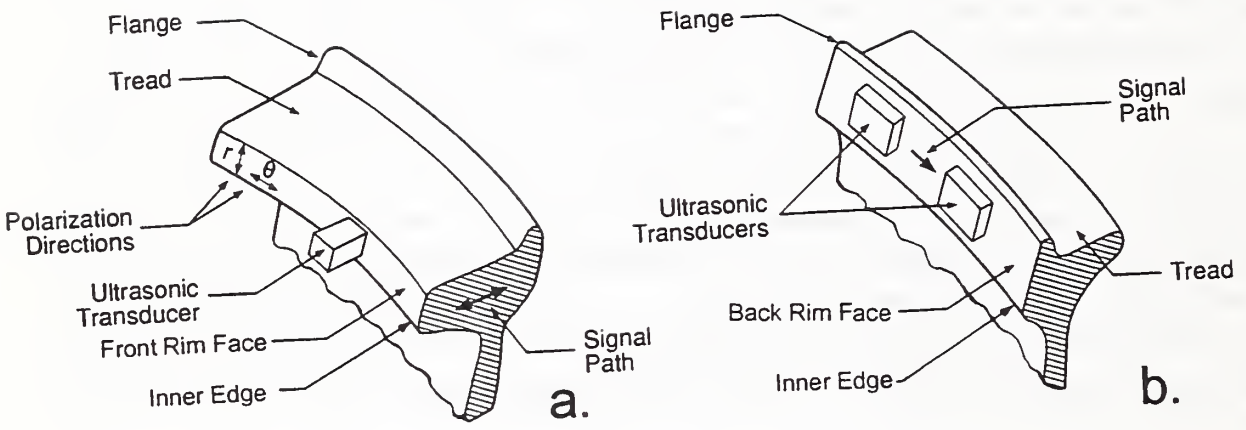

Fig. 1. Wheel geometry showing transducer placement on:
a. frf. b. brf.

The metallurgical texture introduces a birefringence B_0 in the unstressed state. Because casting causes thermal gradients on cooling, it is reasonable to expect that in the rim, radial and hoop directions are (locally) material symmetry axes. Furthermore, if no shear stresses are present in the rim, then σ_θ and σ_r are principal stresses, so that

$$B = B_0 + C_A(\sigma_\theta - \sigma_r), \tag{3}$$

where C_A is the material-dependent, stress-acoustic constant determined from applied stress mechanical tests.

Two questions need resolution: (1) Are the material symmetry axes and the principal stress axes coincident? (2) Since the birefringence measures the quantity $\sigma_\theta - \sigma_r$ and only σ_θ acts as a crack driving force, what is the effect of σ_r on the measurement?

To answer the first question we measured TOFs at various radial locations on our wheels while rotating the shear wave polarization. We found that the TOFs generally have maxima or minima within ±15° of the r and θ directions. The result of rotation between principal stress and material symmetry axes is small when calculating stresses and smaller than the scatter in measurements of B_0 from a population of unstressed rimblocks (described later).

To answer the question concerning the effect of σ_r, consider the stress equilibrium of a cylindrical element for zero shear stress:

$$\frac{\partial \sigma_r}{\partial r} + \frac{(\sigma_r - \sigma_\theta)}{r} = 0 \ . \tag{4}$$

Note that σ_θ vanishes when σ_r is zero; thus, a nonzero radial stress is necessary for the presence of a crack-driving stress σ_θ. However, for large r, only a small σ_r is necessary; to have nonzero σ_θ, the only requirement is that $r\partial\sigma_r/\partial r$ be finite.

We can integrate eq (4), from r_0 to r, where r_0 = radius of tread, and r is the radius where our measurement of stress is to be made. We use the mean-value theorem of integral calculus, and the fact that on the tread σ_r is identically equal to zero. We obtain

$$\sigma_r \cong \frac{1}{r_0} (r_0 - r)\beta\sigma_\theta \ , \tag{5}$$

where β is of order unity. So we have the approximation

$$\sigma_\theta - \sigma_r \cong \sigma_\theta \left[1 - \beta\left(\frac{r_0 - r}{r_0}\right)\right]. \tag{6}$$

For typical locations on the rim, $(r_0 - r)/r_0$ is ~ 0.03. Thus $\sigma_\theta - \sigma_r$ is only slightly less than σ_θ. This discrepancy is much less than other uncertainties in our measurement of residual stress.

Equation (6) is based on plane stress analysis (we assume thickness-averaged stresses). However, the birefringence measurements are sensitive to thickness-averaged stress, so it is consistent to use a plane stress analysis to estimate the effect of σ_r.

3.2 Surface-Skimming Longitudinal and Shear Waves for Surface Stress

The acoustoelastic constant depends on wave type and propagation direction with respect to the stress direction, as well as the material. The highest velocity changes due to stress are for longitudinal waves propagating parallel to the stress direction. For low carbon steel, a stress of 10 MPa means a velocity change of approximately 0.012 percent. In contrast, for a shear wave propagating in the same direction the velocity change amounts to approximately 0.001 percent [19]. The velocity change has the form

$$(V_s - V_r)/V_r = (t_r - t_s)/t_s = C_F\sigma. \quad (7)$$

where V_s and V_r are velocities in stressed and stress-free (reference) states, respectively;
t_s and t_r are TOFs in stressed and stress-free states;
C_F is the acoustoelastic constant for surface waves traveling on the face; and
σ is the stress.

Both longitudinal and shear waves can be SSWs that propagate along the specimen surface. This enables us to make measurements of stresses in a thin top layer of the material. Stress evaluation with subsurface waves is similar to using resistance strain gages; i.e., both measure stresses near the surface.

To find the stress from the measurement of the velocity V_s it is necessary to know the value of the acoustoelastic constant C_F and the value of V_r. Velocity changes during a tensile test will yield C_F, but difficulties arise in determining V_r because of local differences in elastic properties between the test specimen and the stress-free reference sample. Such differences can occur even in the same piece of material [20].

Due to the extremely low sensitivity of shear wave propagating in the uniaxial stress direction, the travel times of shear waves with and without stress are approximately equal. Hence, local changes of shear wave travel time relate to the differences of elastic modulus [21] and temperature.

The travel time difference Δt_L of longitudinal waves in a stressed material and in a reference (unstressed) piece of the same material is the sum of the travel time difference Δt_{Ls} due to stress, the travel time difference due to the dissimilarity of elastic properties Δt_{Le}, and the travel time increment Δt_{LT} due to a temperature difference between the stressed and reference material. Assuming a common temperature, we have

$$\Delta t_L = t_{Ls} - t_{Lr} = \Delta t_{Le} + \Delta t_{Ls}, \quad (8)$$

where t_{Ls} and t_{Lr} are travel times of longitudinal waves measured in stressed and stress-free material. For a stress-free specimen, the travel time t_{L0} will be

$$t_{L0} = t_{Lr} + \Delta t_{Le}. \quad (9)$$

The value Δt_{Le} is a correction for the difference in elastic properties between the test material and the reference material. Generally, the elastic moduli will vary due to changes in texture. However, in isotropic soilds (no texture), there is a relation between longitudinal and shear wave velocities

$$\rho\left[V_L^2 - \frac{4V_S^2}{3}\right] = K. \tag{10}$$

Here K is the bulk modulus, ρ is the density, and V_S is the transverse (shear) wave velocity. Assuming that the bulk modulus is the same for reference and test materials, we have

$$\Delta V_{Le} = \frac{(4V_S\Delta V_S)}{(3V_L)}. \tag{11}$$

When the travel times of longitudinal and shear waves are measured over the same distance, we obtain an expression describing the texture-induced changes of longitudinal wave travel time in terms of changes in transverse wave travel time

$$\Delta t_{Le} = (\frac{4}{3})\times\left(\frac{t_L}{t_S}\right)^3\Delta t_S. \tag{12}$$

Here, we have used relations such as $\Delta t_{Le} = -(d/V_{Le}^2)\Delta V_{Le}$, etc. The final formula for stress calculation is

$$\sigma = \frac{\left[t_{Lr} + A\left(\frac{t_{Ls}}{t_{Ss}}\right)^3(t_{Sr} - t_{Ss}) - t_{Ls}\right]}{C_A t_{Ls}}, \tag{13}$$

where C_A is the acoustoelastic constant for longitudinal surface waves, t_{Lr} and t_{Sr} are travel times of longitudinal and shear waves in a stress-free reference material. These are all experimental values for a given type of material. The coefficient A depends on the ratio of the distances over which both longitudinal and shear waves travel, and depends on the design of the probe head. When the waves travel the same distances, A = 4/3, ignoring diffraction (beam spread).

3.3 Calibration Specimens

Finding B_0 is a crucial point for practical application of the birefringence method. In theory, there are two ways to calibrate: (1) Measure birefringence of a stress-free block made of the same material as the test wheels. (2) Use a wheel with known stress (stress either measured with different techniques or calculated). In our case only the first approach was possible. (There are calculations of stress distributions and values for new, as-manufactured wheels [22], but with a different geometry from that used here.)

The Transportation Technology Center (TTC) in Pueblo, Colorado, provided a set of 20 rimblocks, 2 each from 10 used wheels. All specimens were from the same wheel manufacturer. The block pairs were from circumferential locations 180° apart. The initial B_0 measurements were on the blocks as received and we assumed that saw cutting had relieved any hoop stresses in the wheels. This is valid at the saw cuts (boundary condition $\sigma_\theta = 0$ there), and, if the stress gradient is small, it is true in the bulk of the rimblock. Obviously, the smaller the wedge angle of the block, the smaller is any remaining stress in the rimblock. (These were about 200 mm long at the tread.) Also, if $\sigma_\theta \approx 0$, then for the axisymmetric stress state, $\partial\sigma_r/\partial r \approx -\sigma_r/r$; since $\sigma_r = 0$ on the tread, $\sigma_r \approx 0$ near the tread region of the rimblock. Unless there is a large gradient $\partial\sigma_\theta/\partial\theta$, we may assume that the rimblocks are approximately stress-free in the region of the birefringence measurements. As an experimental test, one from each pair underwent a stress relief heat-treatment (550° C for 8 h and oven-cooled overnight). The average B_0 values of these ten blocks and their standard deviations are in Fig. 2. Comparison with as-received rimblock data showed that, on average, little had changed.

The EMAT measurements on all 20 blocks were a function of radial position on the rim. The index is the inner edge of either the front rim face (frf) or the back rim face (brf), as in Fig. 1. Locations closer to the tread are more positive; those closer to the hub are less positive. With our EMAT (Fig. 3), we had four possible ways of measuring birefringence: (1) Use the bottom coil only and rotate to θ- and r-directions. (2) Use the top coil in the same way. (3) Use both coils, one generating θ-polarization, the other generating r-polarization. (4) Interchange roles of both coils. These serve as internal consistency checks, since B should be independent of method. The data in Fig. 2 show that the average values $\overline{B}_0(r)$ for the four methods agree with each other within our estimated standard deviation of 3×10^{-4}. Figure 2 shows that the average B_0 is approximately constant near the center of rim, and has small gradients near the edges of the rim.

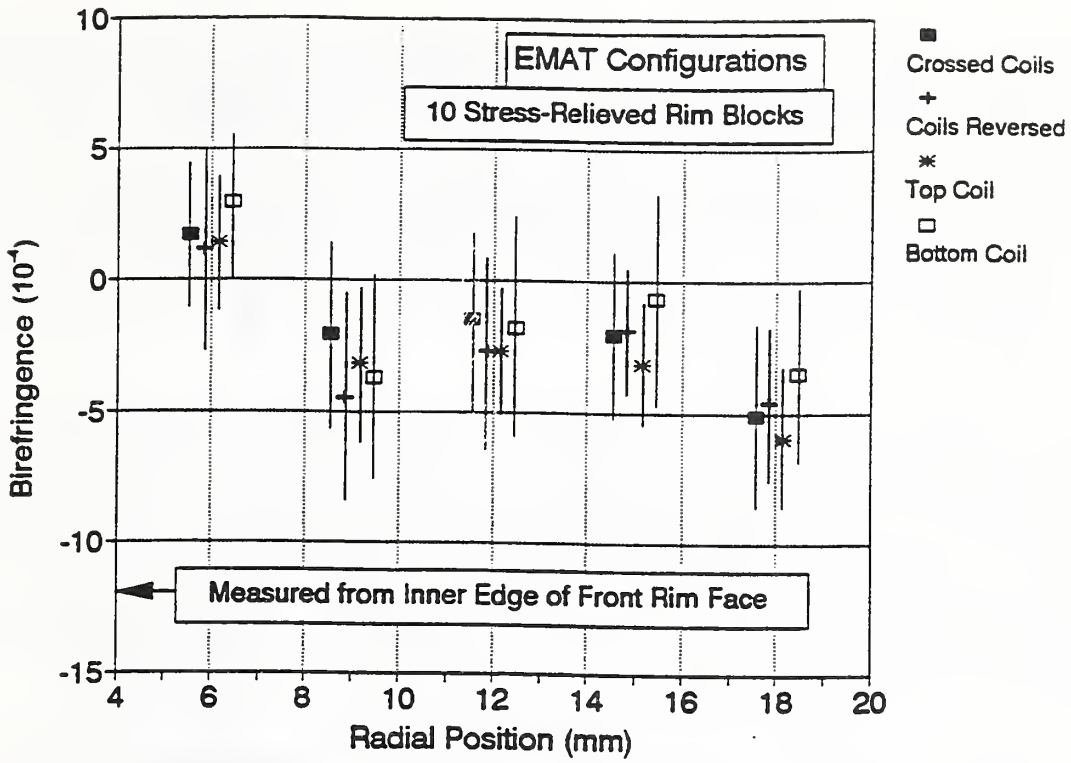

Fig. 2. Average and standard deviation of birefringence due to texture in stress-relieved rimblocks. An EMAT was placed on the frf at five radial locations relative to the inner edge (see Fig. 1). The two EMAT coils (see Fig. 3) were used in four combinations.

For completeness, B_0 was also measured at the center of the frf with the PET system, using a different transduction mechanism than EMATs. The PET $\overline{B}_0$ was in good agreement with the EMAT values.

Error bars in Fig. 2 denote the standard deviation SD of the measurement. The uncertainty in $\sigma_\theta - \sigma_r$ due to variations in material properties, as measured by the SD of B_0, is, from eq (3),

$$\Delta(\sigma_\theta - \sigma_r) = \frac{SD}{C_A}. \tag{14}$$

For $C_A = -7.8 \times 10^{-6}$ MPa^{-1} [13] and a typical SD shown in Fig. 2, we estimate $\Delta(\sigma_\theta - \sigma_r)$ to be about ±50 MPa for our rimblock population.

Measurements of B_0 on the brf were slightly different from frf values. The reason for this may be beam spread (diffraction) as the signal travels through the rim thickness. A small portion of this beam may reflect from the tread surface and interfere with the main lobe of the beam. Such interference could cause small TOF shifts. However, for the same geometry these shifts will be the same (for a given polarization) for the reference sample and for the induction-heated wheels. With the computation of the difference $B - B_0$, these TOF shifts will cancel provided we use consistent B_0 values. For example, we use frf values of B_0 when we measured the birefringence from the front rim face.

In our set of 20 rimblocks, we had 10 (2 each from 5 wheels) from the same plant that made the induction-heated wheels. Upon examination of PET and EMAT data we found the rimblocks from three wheels had B_0 values that were extremely close. The rimblocks from the other two wheels had B_0 values that scattered more. Therefore, in what follows, we use the average B_0 value from the three similar rimblocks (Table 1). Obviously, this points to the need to make a more comprehensive set of measurements of B_0 on a large, statistically significant rimblock population.

The TTC provided another block, numbered as 46726, that received the same stress relief. The block was long enough to use for SSW calibration from a wheel type similar to the 10 wheels under test. The only difference was that the test wheels were single wear wheels and the stress-free block was from a multiple-wear wheel with a thicker rim. Such geometry difference should not result in any acoustic properties changes seen by SSWs. The signals move through a thin surface layer of wheel steel composed of dendritic grains oriented perpendicular to the surface (Figs. 19 and 20 of Ref. [15]).

3.4 Acoustoelastic Coefficients for Cast Wheels

Previous studies on American cast wheels have determined the acoustoelastic coefficients. The values in Table 2 are for shear waves propagating in the direction perpendicular to the stress direction, C_A, and longitudinal waves propagating along the stress direction, C_S.

Table 1. Values of B_0 ($\times 10^4$) for both frf and brf measurements.

	EMAT	PET
frf	-2.2	-3.5
brf	-3.8	-4.6

Table 2. Listing of acoustoelastic constants.

Wheel Type/ Manufacturer	C_A 10^{-6} MPa^{-1}	C_S 10^{-6} MPa^{-1}	Ref.
Cast/Griffin	-7.6		7
	-7.8*		12
		-13.5	11
Cast/Southern	-9.5	-14.7	12
Forged	-7.9	-12.5*	10

* These are the constants used in our calculations.

4. ULTRASONIC SYSTEMS FOR RESIDUAL STRESS MEASUREMENT

4.1 Piezoelectric Transducers (PETs)

The standard PET for measuring the birefringence had a single element (piezoelectric crystal) measuring 12 mm × 12 mm and operating at 2 MHz. The crystal is cut to generate a shear wave. Rotating the probe head changes the direction of shear wave polarization. The acoustic couplant was a small amount of (uncured) epoxy resin.

TOFs for all PET measurements used the first and second echoes reflected from the opposite rim face; an operator set a cursor on the first cycles in the two echoes. The difference between first and second echoes partially compensates for the effect of couplant thickness. To a first approximation the couplant merely adds an additional acoustic path length, with an additional TOF. This is the same for both echoes, so taking the difference in their TOFs removes this artifact. However, the second echo limits how close to the tread it is possible to make a measurement, since beam spread effects, larger in the second echo, can cause errors in TOF.

A second PET (called the multitransducer probe head) operates at 2.5 MHz. It contains several crystals transmitting and receiving SH waves. There is no need to rotate this probe head to measure TOFs for radial and hoop polarizations. Birefringence measured with this system is averaged over a larger volume of rim material compared with the single-transducer PET.

A third PET (used for birefringence in selected wheels) operated at 4 MHz with a 7 mm × 7 mm element. The aim of measurements with this probe head was to check for any change in birefringence due to a different frequency and beam divergence.

Measurements of TOF for surface-skimming longitudinal and shear vertical waves used a multitransducer, linear probe head. Using two sets of transducers eliminates the influence of surface roughness on readings by measuring the time in both directions and averaging. This probe head has a temperature sensor to correct TOFs for both pressure and shear waves automatically. All measured times are corrected to the same temperature. (Ultrasonic velocity varies with temperature; a change in temperature of a few degrees Celsius produces velocity changes that are the same order of magnitude as those produced by the stresses in the wheels. This is not important for birefringence measurements where all measurements occur in a matter of seconds.)

Piezoelectric crystals mounted on wedges generate SSWs. The sound waves pass through the wedge and an oil or water-based acoustic couplant. Since the sound speed in the wedge is lower than that of the cast steel the wave refracts according to Snell's law. The wedge angle is chosen so that the angle of refraction is parallel to the wheel surface. The wave propagates in a region close to the wheel surface over a path about 200-mm long. Another (receiving) wedge intercepts part of the wave from the wheel surface and refracts it into a detector.

All probe heads were attached to the portable ultrasonic stress meter. This device has the electronics to transmit and receive the ultrasonic waves and a microprocessor to make TOF readings and calculate stress values. Both probe heads and meter were developed at the Institute of Fundamental Technological Research, Polish Academy of Sciences. A description of the stress meter and its operation is in Ref. [23].

4.2 Electromagnetic-Acoustic Transducers (EMATs)

A permanent magnet EMAT operating at 2 MHz (Fig. 3) measured the birefringence. A shaped polepiece increases the magnetic induction of the magnet. This probe head has two stacked, flat (pancake) coils whose axes are perpendicular to each other; they generate shear waves with hoop (θ) and radial (r) polarizations, respectively. We refer to a bottom and top coil; the former is closest to the wheel. We switch between EMAT coils to generate the θ- and r-polarizations of the shear wave instead of rotating the transducer.

The crossed-coil EMAT had a fixture with an edge-finder to locate the inside edge of the frf and use it as fiducial mark for the radial location [15]. We estimate that this allows repetition of the position with less than 1 mm uncertainty during scanning around the wheel circumference. The current fixture design will not allow it to work on the brf, so it became necessary to hand-place the EMAT (as was the case with all PET measurements).

TOFs were from the first echo reflected from the opposite rim face [15]. When the pulser energizes the EMAT coil, a simultaneous START signal goes to a counter. A special digital delayed gate circuit detects a zero-crossing in the returning echo and sends a STOP signal to the counter [9]. The counter displays the time difference between the two signals and transmits the number to a small computer. Simple software then calculates both birefringence and stress.

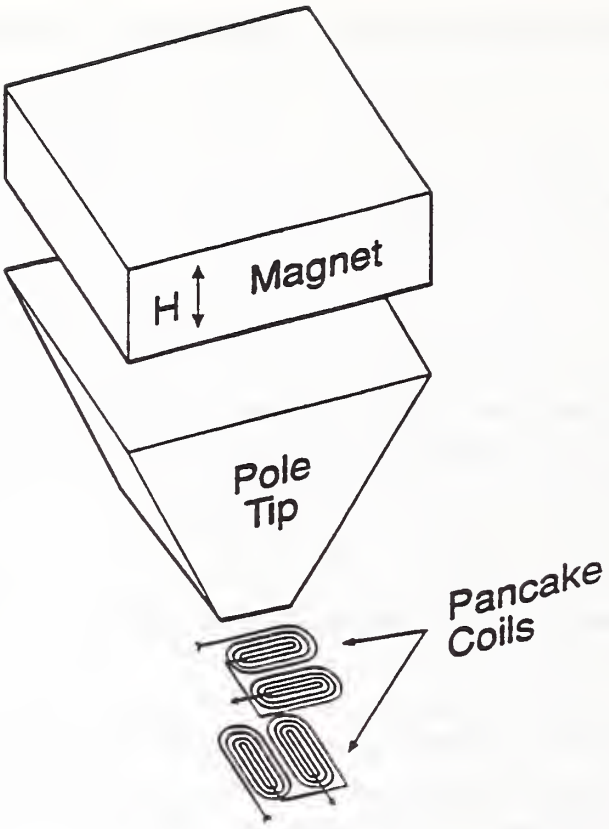

Fig. 3. Schematic of EMAT used for birefringence measurements. The two stacked orthogonal coils are flush to the pole tip.

5. TEST SPECIMENS

The test specimens were 10 railroad wheels cast in the same production run. They were curved plate, class C, and heat-treated. The 10 risers used for pouring the metal into the molds were still visible and became the circumferential reference marks (Fig. 4). The dendritic grain structure near the surface should be very similar to that of similar wheels we have examined in the past [15].

Two wheels remained in the as-manufactured condition. The other wheels received inductive heating to simulate heat loads seen during braking. The induction coil was very close to the wheel tread; during heating the hub supports the wheel. Powers are in Table 3.

Heating time for all wheels was 30 min. The assumption is that the heat and associated stresses in the rim are axisymmetric. As manufactured, the residual hoop stresses created

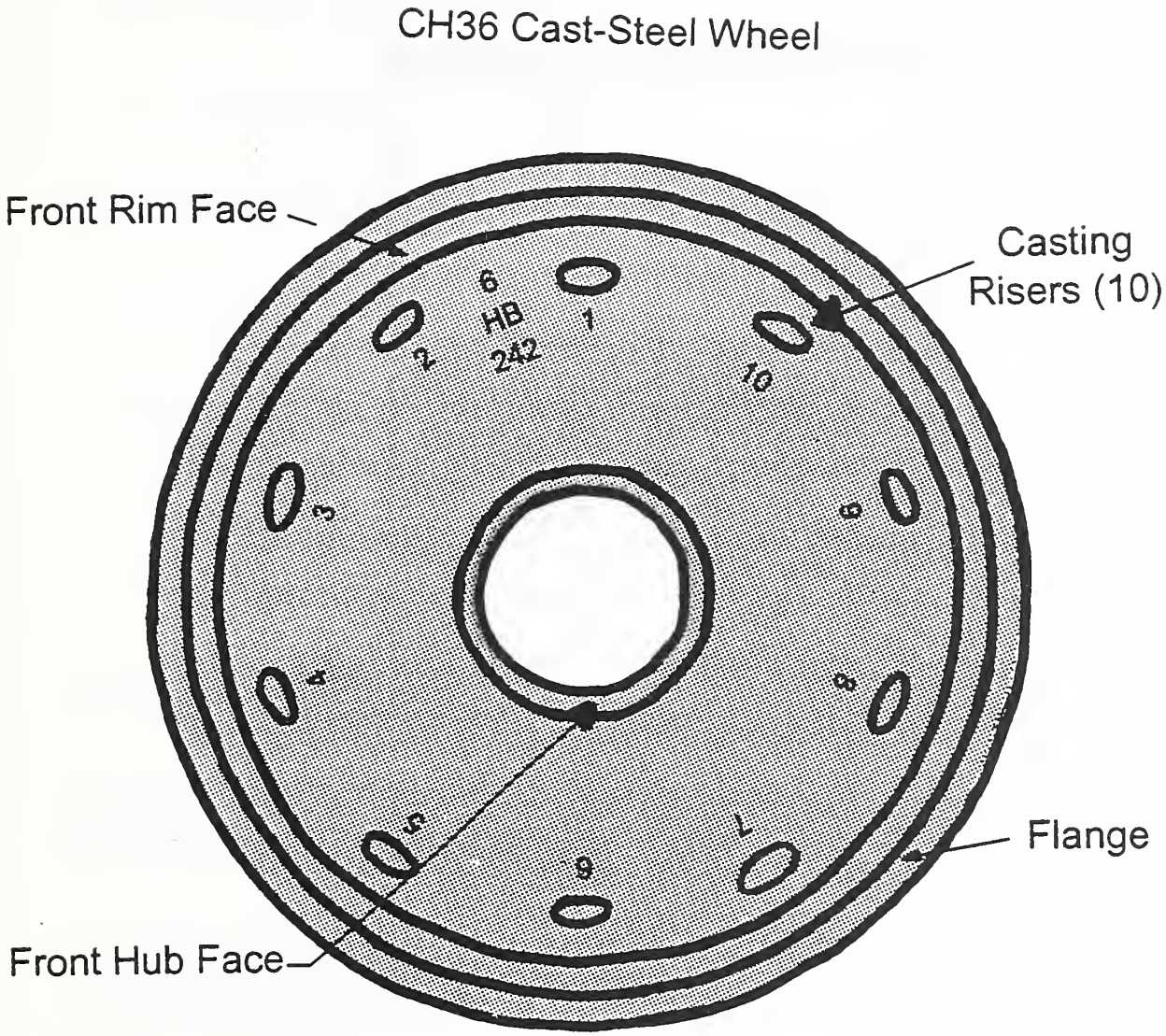

Fig. 4 Sketch of the front (outside) of our test wheels. The numbered casting risers were the circumferential index marks.

Table 3. Induction power in test wheels.

Inductive heating power kW (hp)	Wheel ID serial number
0	26508 26512
38 (51)	26515 26529
42 (56)	26506 26520 26522
45 (60)	26513 26524 26426

Manufacture date: 01 93
Heat number: 5227
Plant: GK

Pattern number: CH36
Class: C

during quenching with water spray and heat treatment are about −140 MPa [22]. Experience suggested that 38-kW heating would reverse this bulk compressive stress [24]. Higher heating powers would then produce tensile hoop stresses in the wheels.

Shot-peening generated compressive residual stress on a very thin surface layer of the tread. This would have negligible influence on ultrasonic measurements at the frequencies used.

6. SCOPE OF MEASUREMENTS

Measurements on all 10 wheels used transducers on both frf and brf. The inner rim edges on both faces are directly opposite each other (Fig. 1).

The front face measurements were:

- birefringence with an EMAT at a radial location 12 mm from the inner edge of the rim face,
- birefringence with a PET at a radial location 14 mm from the inner edge of the rim face, and
- surface stress with the PET at a radial location with 15 mm between the inner edge of rim face and the middle of the acoustic path.

The back face is much wider. On this face, the measurements were:

- surface stress with the PET at two radial locations: 15 mm and 35 mm from the inner edge of the rim face,
- birefringence with both EMAT and PET at a radial location 14 mm from the inner edge of the rim face, and
- birefringence with the EMAT at 12 mm from the inner edge of the rim face.

There were 20 circumferential locations on each wheel.

With a total of over 1,000 stress measurements, this set of wheels is probably the best characterized in the world.

Rim-face preparation for the PETs was a small amount of hand filing. To check the influence of the surface roughness, a test on wheel 26506 (42 kW) omitted this preparation. In practice, the results were the same.

Birefringence gives stress averaged through the rim thickness. The SSW method gives stress in a surface layer (about 1 mm thick) of the rim face, averaged over the distance between receivers. Because of this long averaging distance, the SSW results are smoother as a function of circumferential position compared to the birefringence results (which average over apertures about 10 mm × 10 mm). Also, the dendritic structure in the rim surface layer is probably more uniform over the circumference than in the bulk of the rim; there the crystallization conditions could be different for regions close to the casting risers and between them.

Ten of the circumferential positions were on the same radii as the casting risers (integers 1 to 10). The other 10 positions (off-riser) were half-way between the risers and identified as 1.5 to 10.5. On all 10 wheels, a manufacturer's mark served as an index (Fig. 4).

7. RESULTS OF MEASUREMENTS

7.1 Birefringence Measurements with PETs

Birefringence measurements with the standard 2-MHz 12 mm × 12 mm PET, are in Figs. 5 a-d. The probe position was the center of the frf so that the distance between probe axis (and the acoustic beam axis) and inner rim edge was 14 mm.

In Fig. 5, the birefringence becomes more negative, on average, with increased induction heating. Consequently, the stresses become less compressive and more tensile. Mean values of birefringence (the average of values at the 20 circumferential locations) and corresponding stresses for each wheel are in Table 4.

Figure 5 shows that the scatter of birefringence in as-manufactured wheels is smaller than in induction-heated wheels. In some wheels, birefringence at positions near the casting risers seemed higher than between them (see for example wheel No. 26515, Fig. 5b). Figure 6 compares these on- and off-riser birefringences. Here the values are the averages from all 10 positions for each wheel of each heat set. The differences between measurements on and between risers are negligible, from a practical point of view. However, the large scatter evident in Fig. 5 shows that several measurements are necessary to obtain good averages.

As mentioned before, the acoustic energy in the sound beam spreads out (diffracts); theoretically, some of it could reflect from the tread and plate area and interfere with the main lobe of the beam (which propagates straight through the rim thickness). For the transducer apertures and frequencies used for the PETs, the estimated influence of side wall reflections on TOFs of the second echo in forged wheels is negligible. However, to test whether there are any such interference effects in cast wheels, we made measurements with the same PET, with waves propagated from front and back rim faces (Fig. 7). While they are not identical, the equivalent average stresses for the two data sets are close. For the PET measurements, we calculated the average frf stress to be −35 MPa (−5 ksi), and for brf to be −52 MPa (−8 ksi).

A further test used two PETs with different apertures, the standard and multitransducer probe heads. Figure 8 shows the circumferential distribution of birefringence measured on as-manufactured wheel, 26512, and on a 45-kW heated wheel, 26526. In both wheels the trend is the same, showing little influence of the geometry of the cast wheel rim on TOF readings.

It is also worth mentioning that birefringence, measured in material with a gradient of texture (e.g., cast wheels), can vary slightly with transducers of different sizes. These variations are a result of birefringence averaging over the volume of material determined by transducer area,

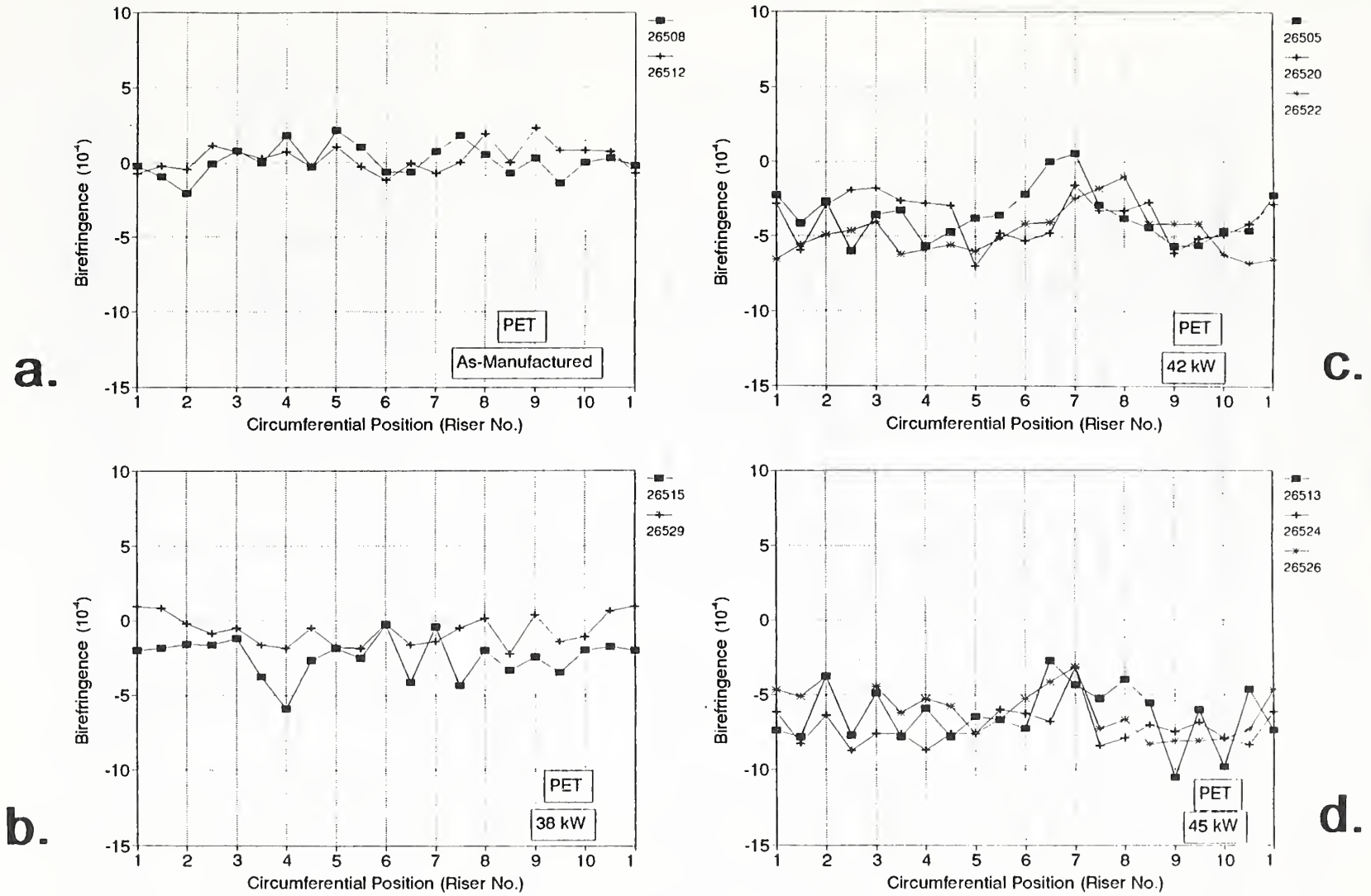

Fig. 5. Birefringence measured with the standard PET on the frf of 10 test wheels.
a. As-manufactured. b. 38 kW. c. 42 kW. d. 45 kW.

Table 4. Mean Birefringences and Stresses Measured with PETs.

Wheel ID (input power, kW)	Mean birefringence ($\times 10^{-4}$)	Mean stress (MPa)
26508 (0)	0.08	-49
26512 (0)	0.29	-49
26515 (38)	-2.49	-13
26529 (38)	-0.78	-35
26506 (42)	-3.69	2
26520 (42)	-3.88	5
26522 (42)	-4.71	16
26513 (45)	-6.35	37
26524 (45)	-7.25	48
26526 (45)	-6.12	34

beam shape, and material thickness. Different transducer sizes change the volumes of material affecting the texture.

Figure 8 also shows how induction heating introduced slight nonaxisymmetric stresses; compare the relatively smooth lines for as-manufactured wheel and the significant scatter in birefringence measured in the 45-kW wheel. The departure from axial symmetry can be due to either variations in stress, or possibly the influence of texture; Eq. 5 shows that the birefringence depends upon both $\sigma_\theta - \sigma_r$ and on B_0. Since the wheels did not exceed the recrystallization temperature [24], texture should not have changed. This means that the variation in B reveals variations in stresses.

Figure 9 presents birefringence measured with a PET on wheel No. 26513 (45 kW) between positions 9 and 9.5 in 20-mm increments. (Note in Fig. 5d a significant change in birefringence measured at these two points.) The almost monotonic change is another indication that the

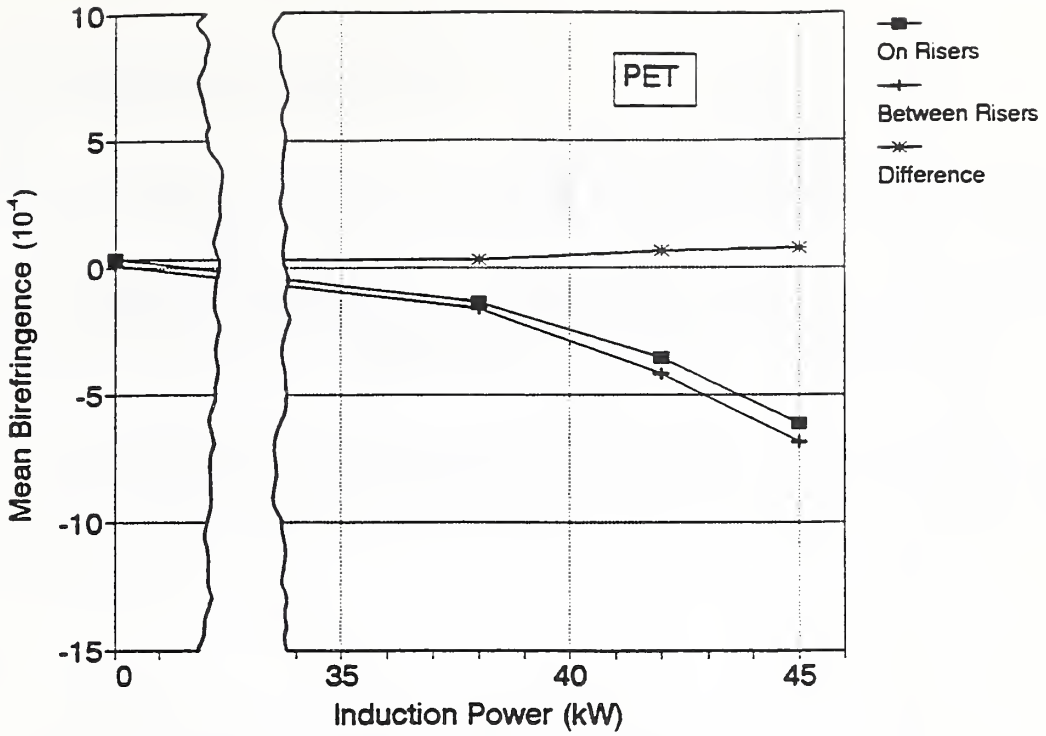

Fig. 6. Comparison of average PET birefringences at on-riser and between-riser locations, as a function of induction heating.

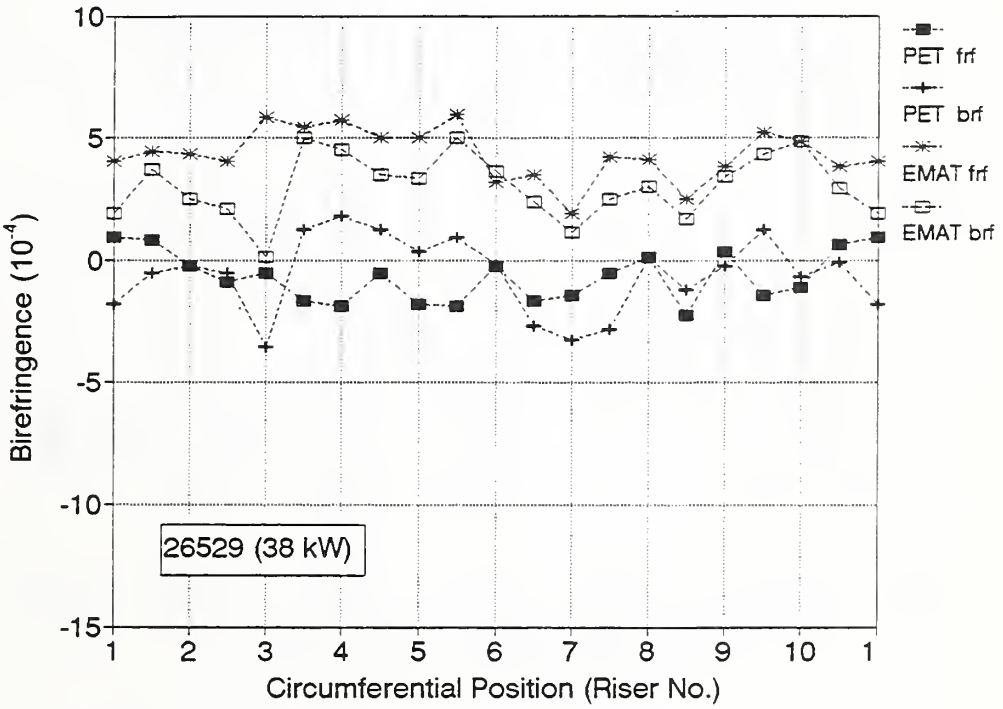

Fig. 7. Comparison of birefringence measured on the same wheel, with the transducers placed on front and back rim faces.

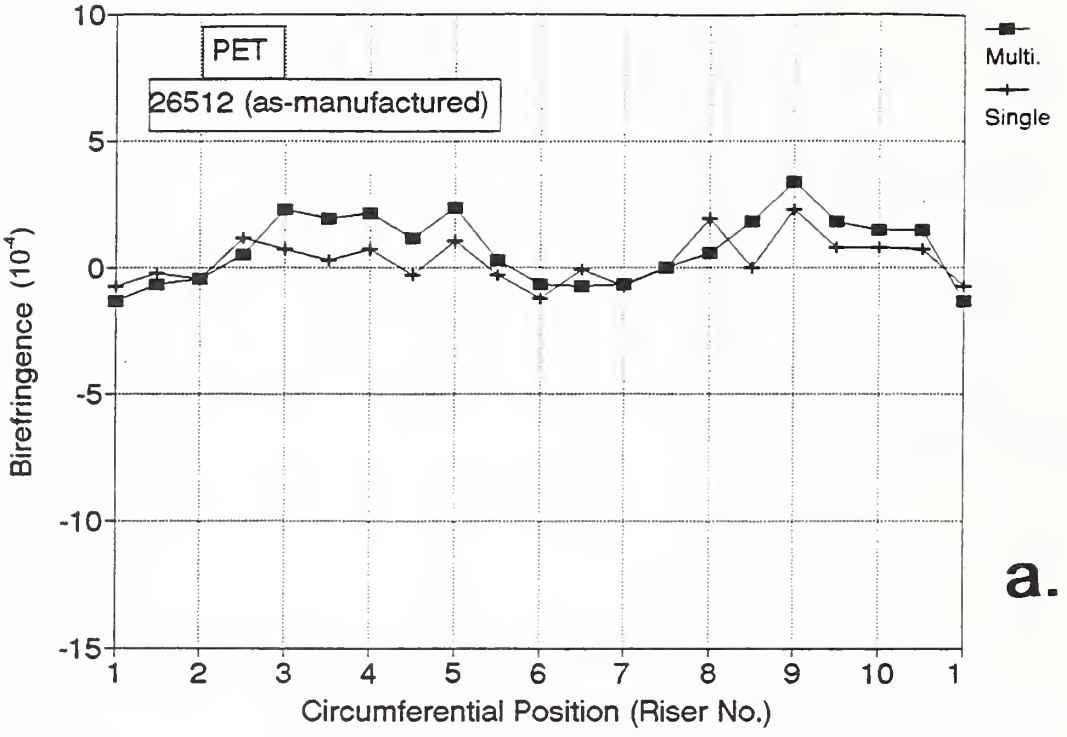

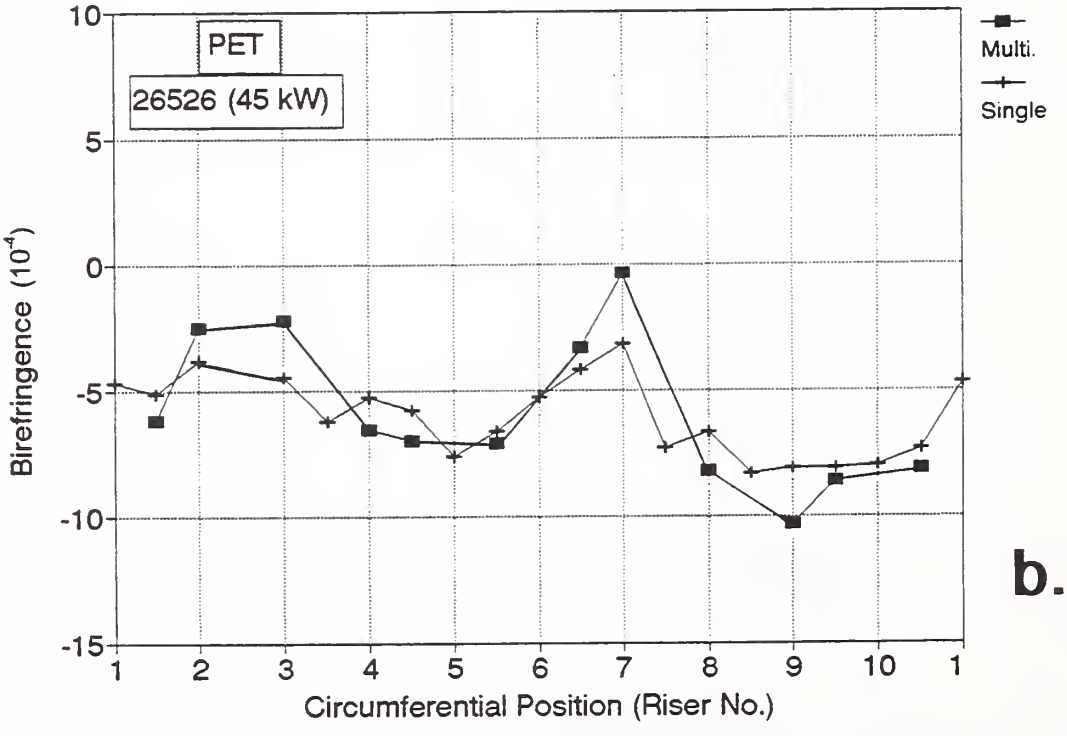

Fig. 8. Birefringence measured with two different PETs on the frf.
a. As-manufactured. b. 45 kW.

scatter in birefringences is not due to measurement uncertainty (which gives a random scatter to the data) but is due to variability in stress.

Figure 10 shows the radial distribution of birefringences measured with various PET probes on the brf of wheel 26524 (45 kW), both on and between casting risers. Radial values of position are increasingly positive going toward the tread, and increasingly negative toward the hub. Data taken between risers have a somewhat smaller radial gradient than data taken on-riser. This trend was the same with all three PETS used in this set of measurements.

The value of $B_0 = -4.6 \times 10^{-4}$ was from the mid-rim position, based on three rimblocks from the same plant that produced the induction-heated wheels. If this value is valid for all radial positions, the data of Fig. 10 show that the stress becomes more tensile toward the tread, and less tensile toward the hub.

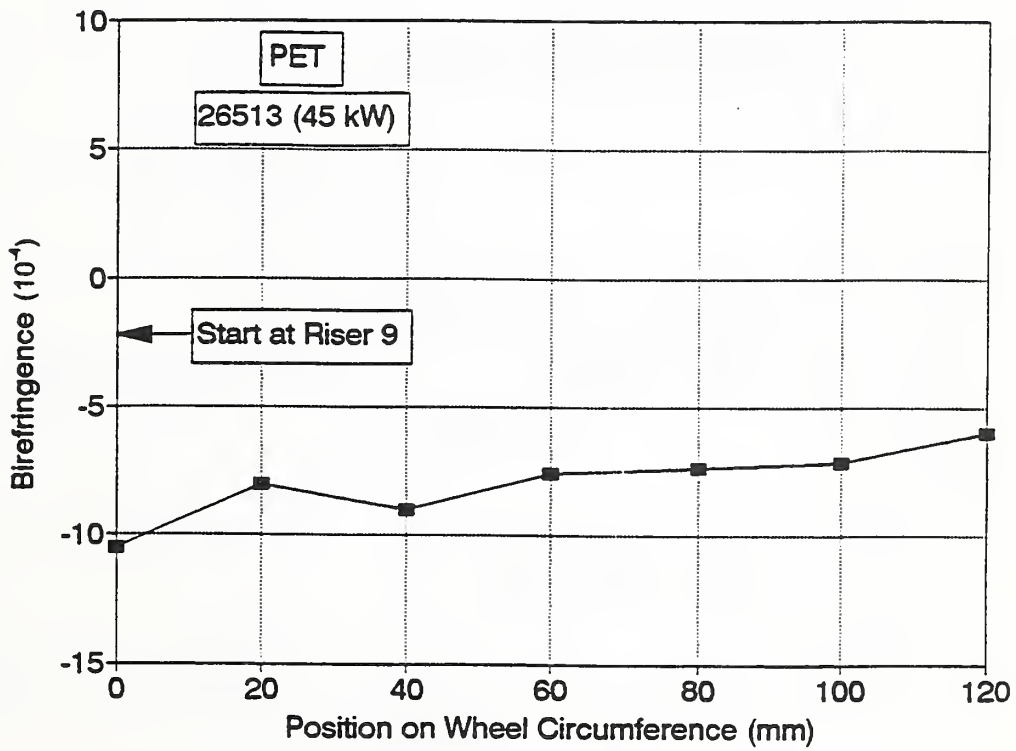

Fig. 9. Birefringence measured with a PET at 20-mm intervals between locations 9 and 9.5 on a wheel subjected to 45-kW induction heating.

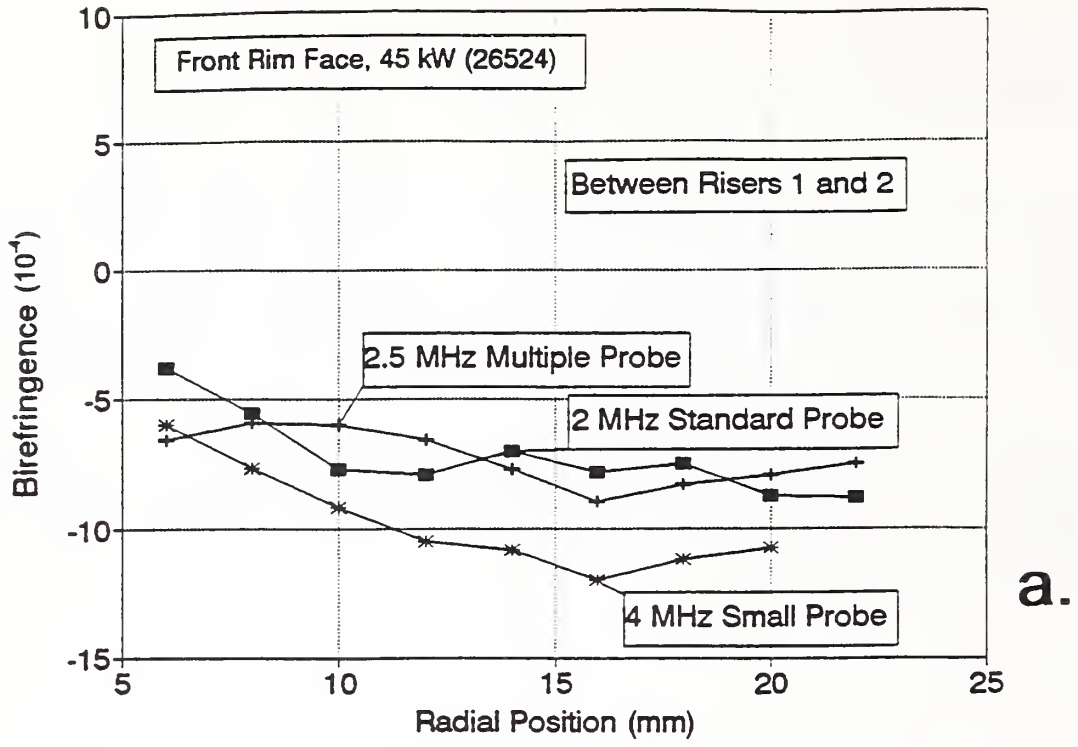

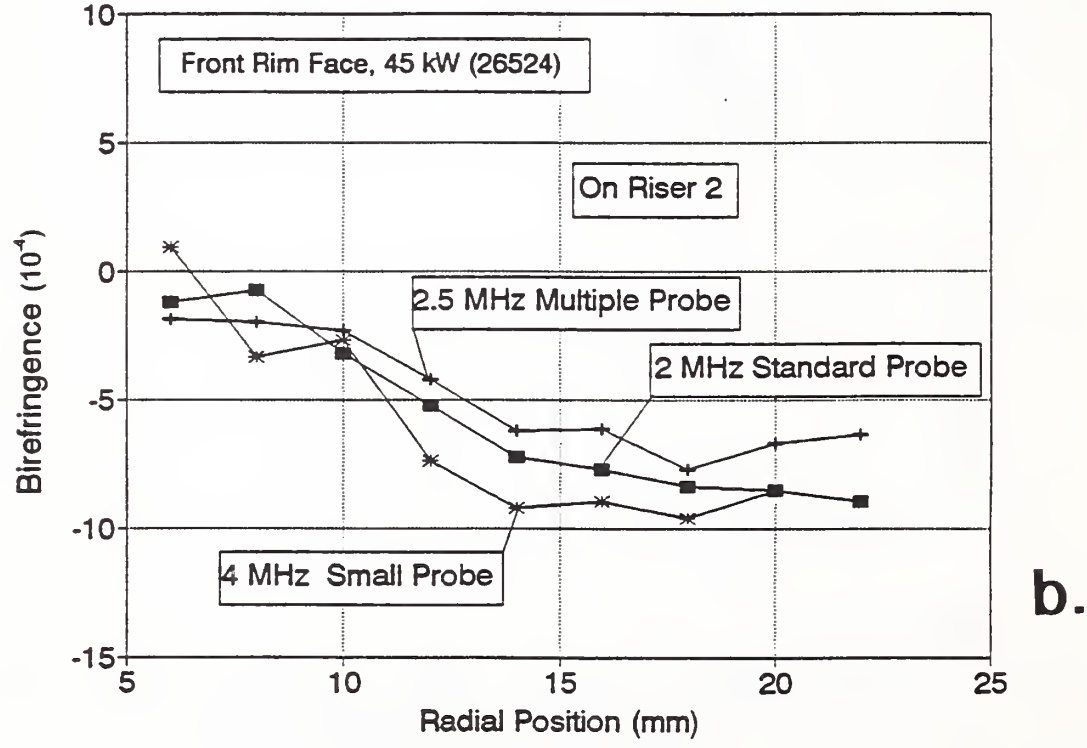

Fig. 10. Radial distribution of birefringence measured with three PET probes on a wheel heated at 45 kW.
a. Location 1.5. b. Location 2.

After the NDE tests, the manufacturer performed DE on three of the heated wheels (see below) and then returned two rimblocks cut from each. We heat treated these for stress relief, as noted above, and made multiple measurements of B_0 with the EMAT system. Figure 11 shows the measurements as a function of radial position on the rimblocks near the saw cuts at risers 2 and 7 on wheel 26529 (38 kW). The general trend is similar to Fig. 2. Again the relatively constant values from 12 to 18 mm indicate the desirable locations for transducer placement. The B_0 numbers show no significant variance from our original calibration specimens (Table I).

Typical sets of values clustered around the saw cuts are in Fig. 12. When the EMAT is on the frf (Fig. 12a) there is a smaller spread with both radial and circumferential positions than on the brf (Fig. 12b). Also, the brf birefringence tends to be somewhat higher than on the frf. From these limited data, the best choice for probe position appears to be at about 14 mm from the inner edge on the frf. On the few points tested, the repeatability was excellent.

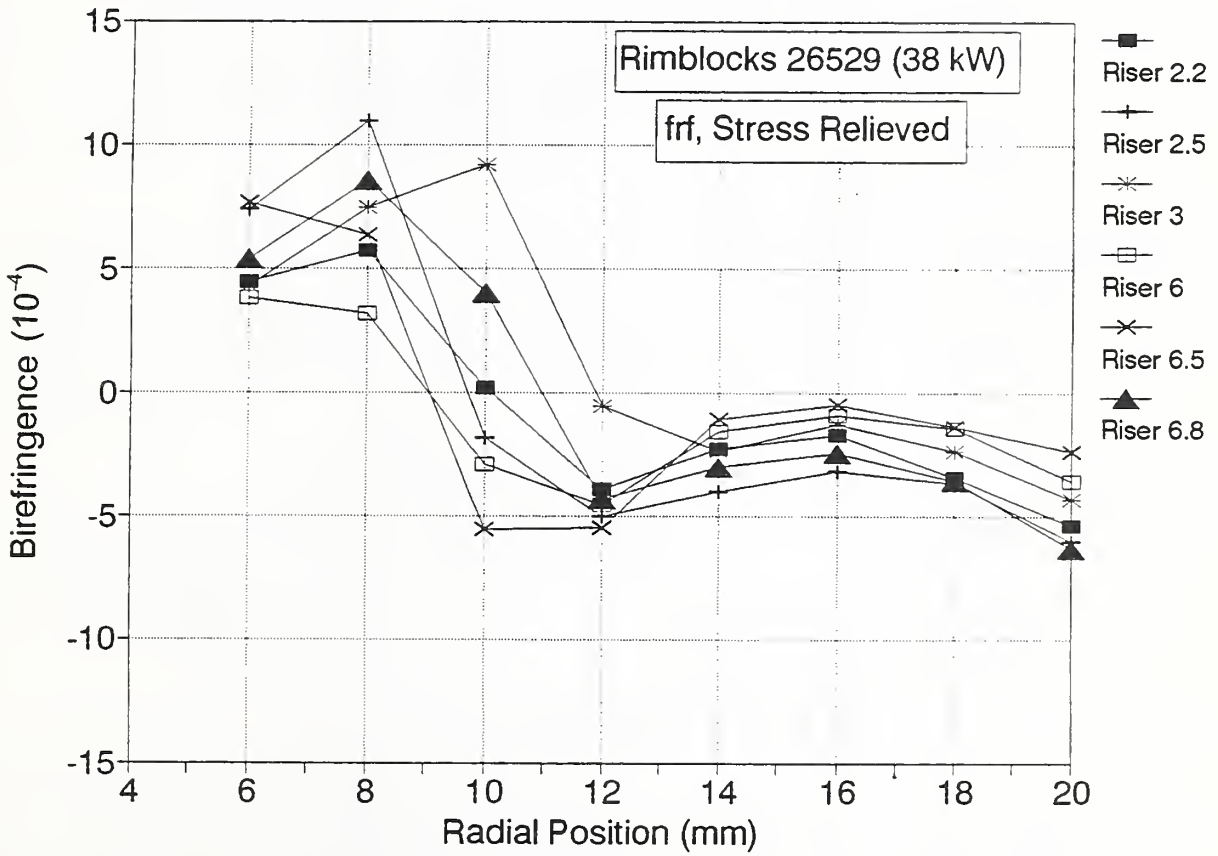

Fig. 11 Radial distribution of birefringence measured with the EMAT on a stress-relieved rimblock cut from wheel 26529 (38 kW).

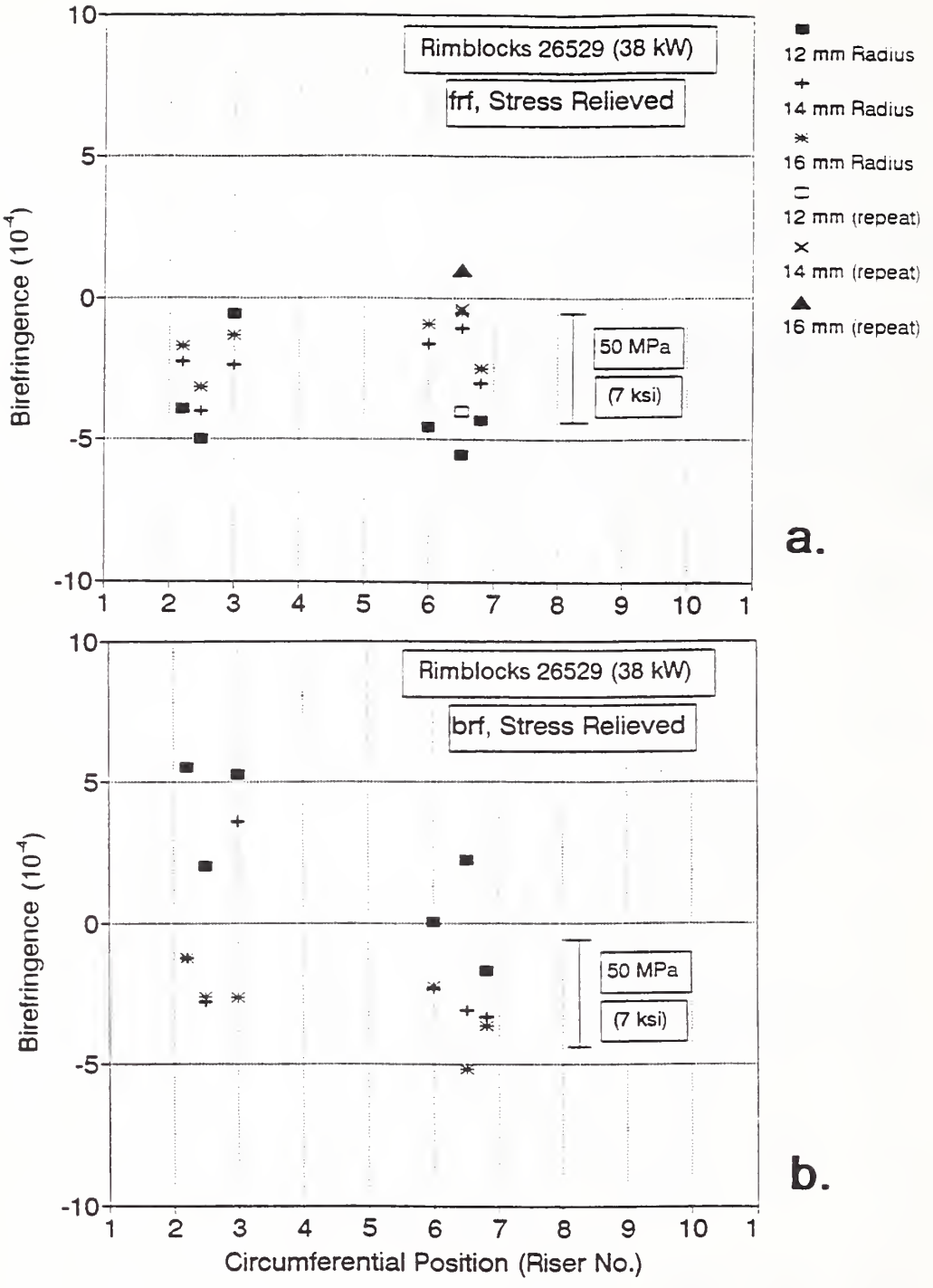

Fig. 12 EMAT measurements of B_0 on a stress-relieved rimblock cut from a heated wheel. The transducer placements were three circumferential positions near each of the two saw cuts made for DE and included three radial values at each.
a. EMAT on frf. b. EMAT on brf.

7.2 Comparison of Two Techniques of Birefringence Measurements

In theory, acoustic birefringence measured with EMATs and PETs in material with uniform texture should be identical. To verify this, we used both systems to measure B in the middle of a large steel plate, 100 mm thick. PET and EMAT results were experimentally the same, showing that, in the absence of sidewalls or gradients, the measured birefringence does not depend on transducer aperture, frequency, or wave generation mechanism. The wheel data in Fig. 13 show an offset between the two systems, with the EMAT giving a value of B approximately 5×10^{-4} higher. However, the data sets (EMAT and PET) are from radial locations 2 mm apart. We will show later that the systems agree within about 2×10^{-4} when they are at the same radial location (14 mm from inner edge of front rim face).

Next, we compare the trends from these two ultrasonic systems both on and off the casting risers. On-riser data in Fig. 14a show a structure with both systems; note that the quasi-periodic variation of birefringence as a function of circumferential position appears in all data sets. In contrast, Fig. 14b shows little structure for birefringence measurements made at locations between casting risers. The same general pattern appeared for all inductively heated wheels (Figs. 15 and 16). The EMAT and PET data replicate each other, apart from an approximately constant offset.

Figure 6 showed that the average PET data for on-riser measurements were close to the average for off-riser data. This is also true for EMAT data. With enough measurements around the circumference, it makes little difference whether we measure on-riser or off-riser. Here the average is over 10 locations for on-riser and off-riser data, so large differences may result for a smaller sample.

Figure 13 shows that EMAT measurements made on frf and brf agree quite well with each other for as-manufactured wheels. The PET values are for comparison. We found that as the heating increased, the frf and brf EMAT measurements began to differ. All measurements show the same trend (e.g., all have local maxima at the same circumferential location), but EMAT brf values are now closer to PET measurements than are the EMAT frf values.

We also measured a subset of the wheels with a second, nominally identical EMAT placed on the brf so that its acoustic axis coincides with that of the PET (14 mm from inner edge of the rim). Rather than switching between coils, we used only the bottom coil and rotated the EMAT. This was to remove any possible artifacts due to: (1) different radial locations for PET and EMAT measurements. (2) Any liftoff changes [25] that might result from use of the fixture [15]. In this case, the EMAT birefringence measurements were now in better agreement with PET measurements. In fact, the average difference between them is now only

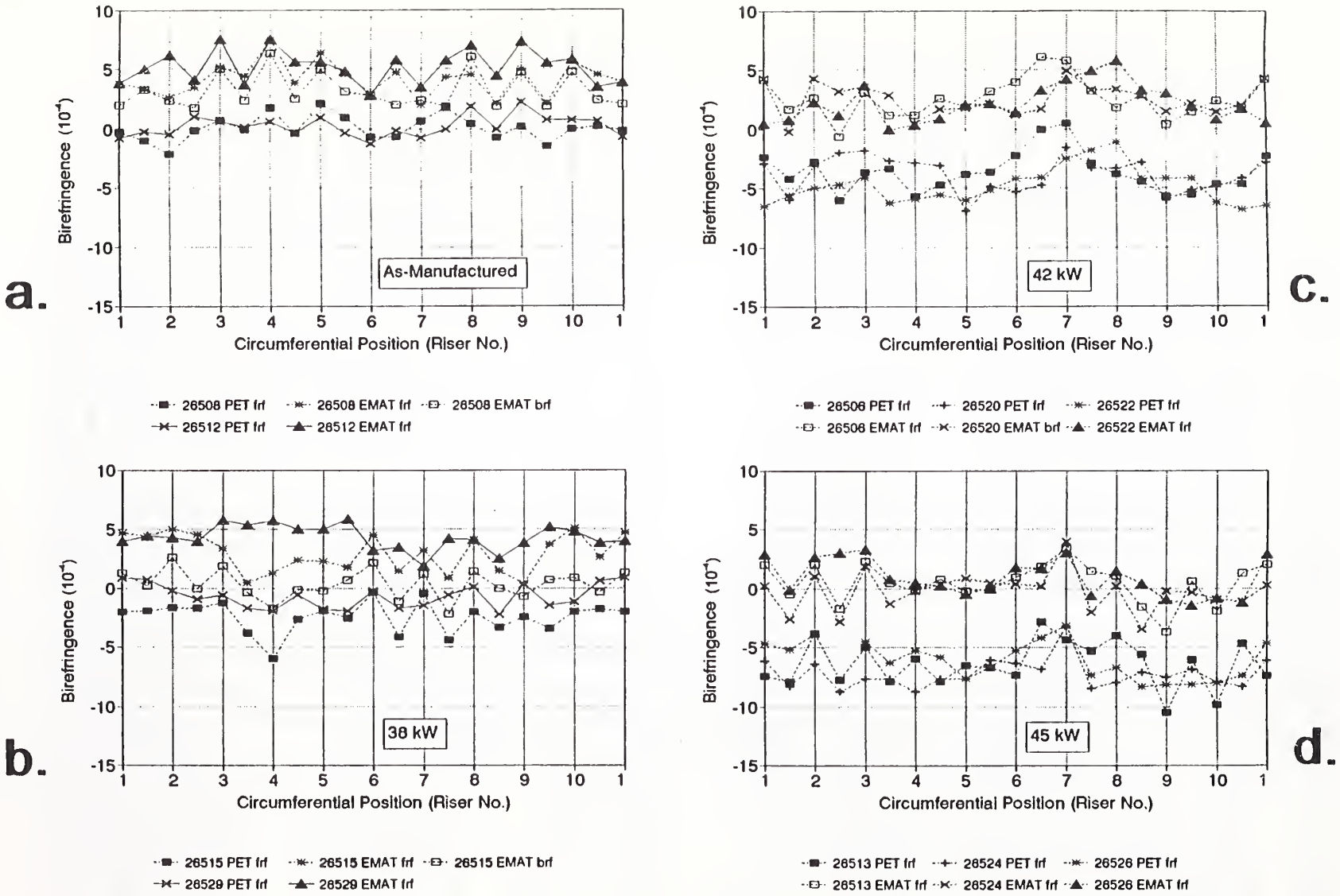

Fig. 13. Birefringence measured on ten wheels using an EMAT positioned on frf and brf and a PET on the frf. EMAT and PET radial positions differ by 2 mm.
a. As-manufactured. b. 38 kW. c. 42 kW. d. 45 kW.

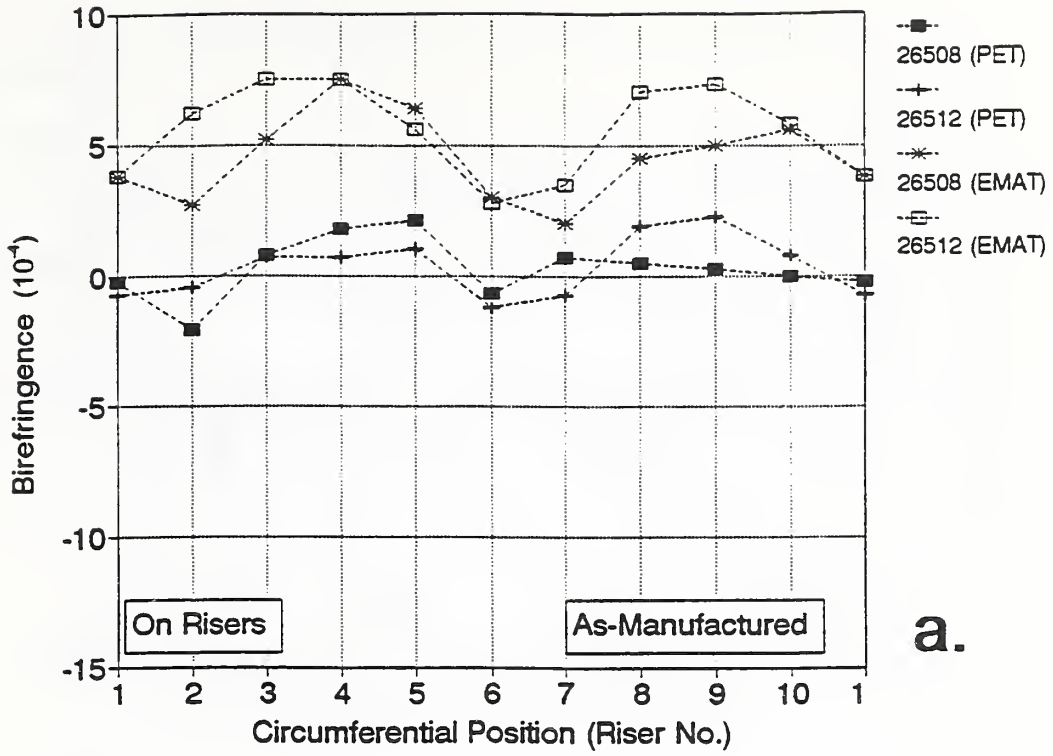

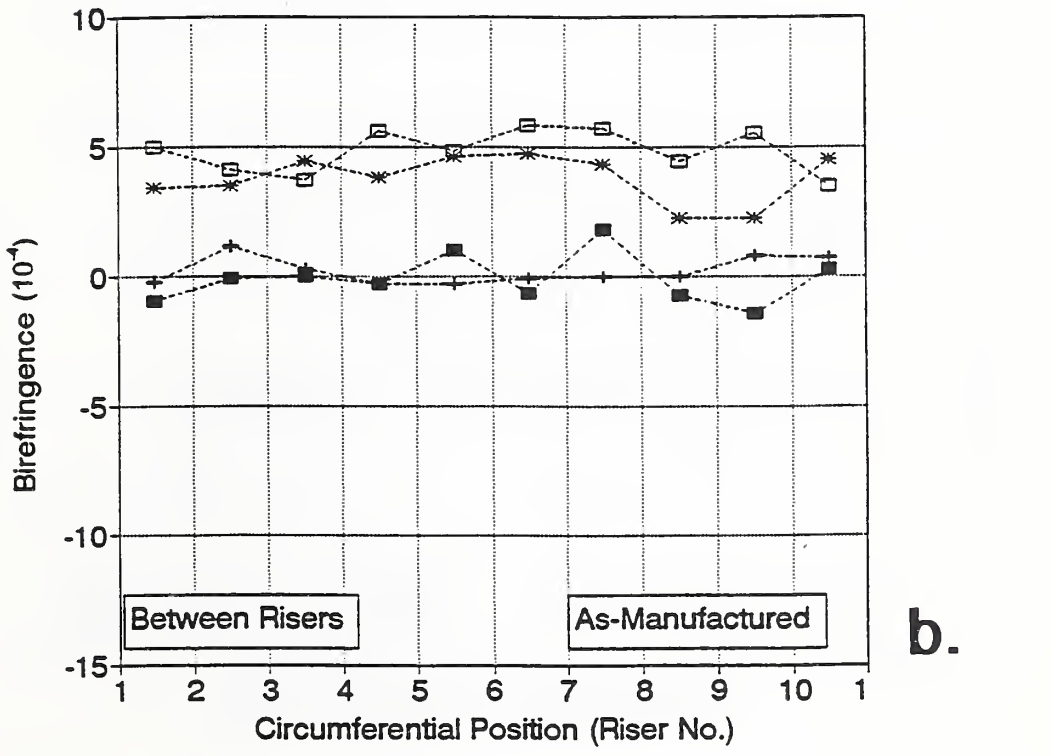

Fig. 14. Birefringence measured with EMAT and PET on as-manufactured wheels. a. On risers. b. Between risers.

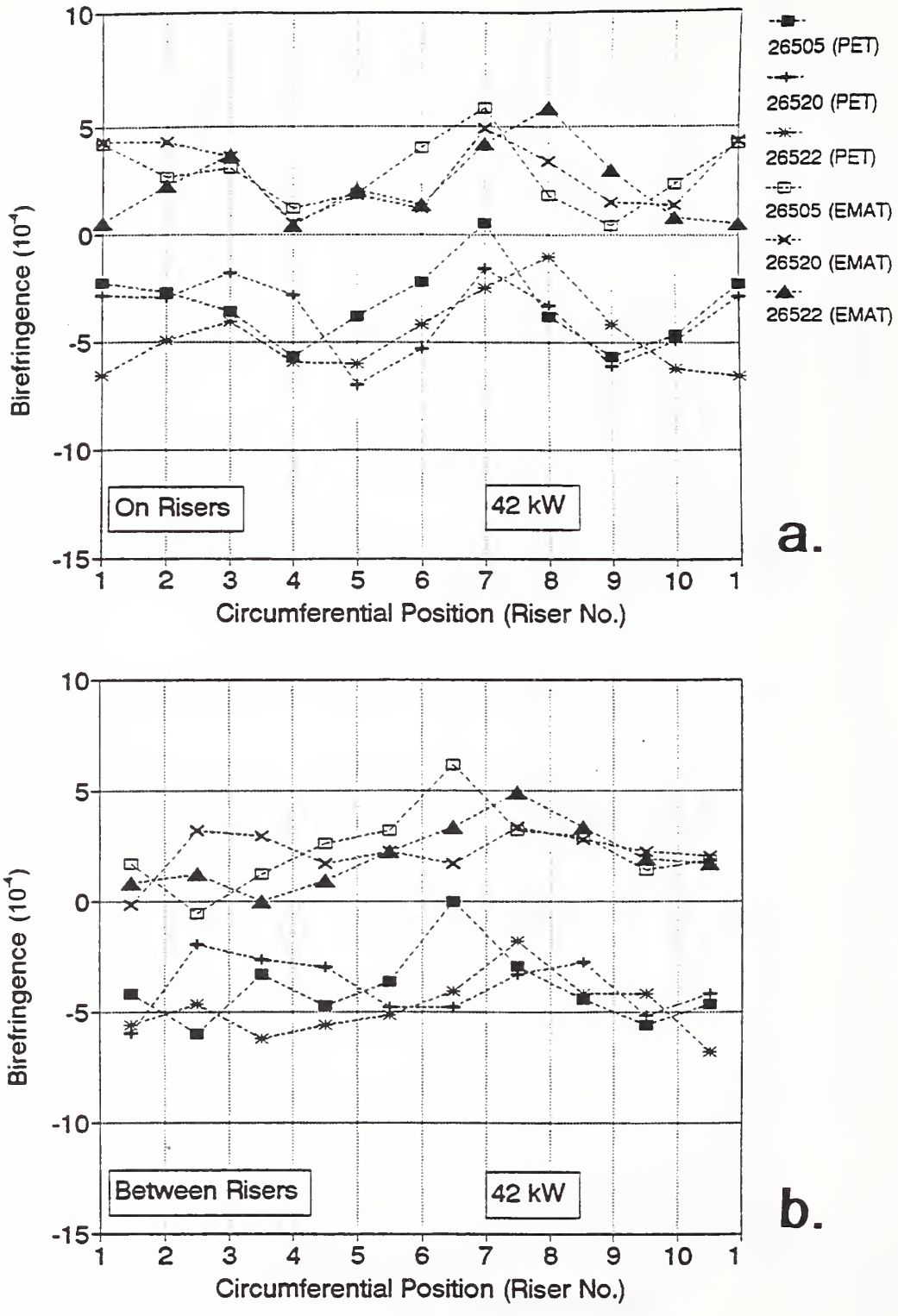

Fig. 15. Birefringence measured with EMAT and PET on 42-kW wheels. a. On risers. b. Between risers.

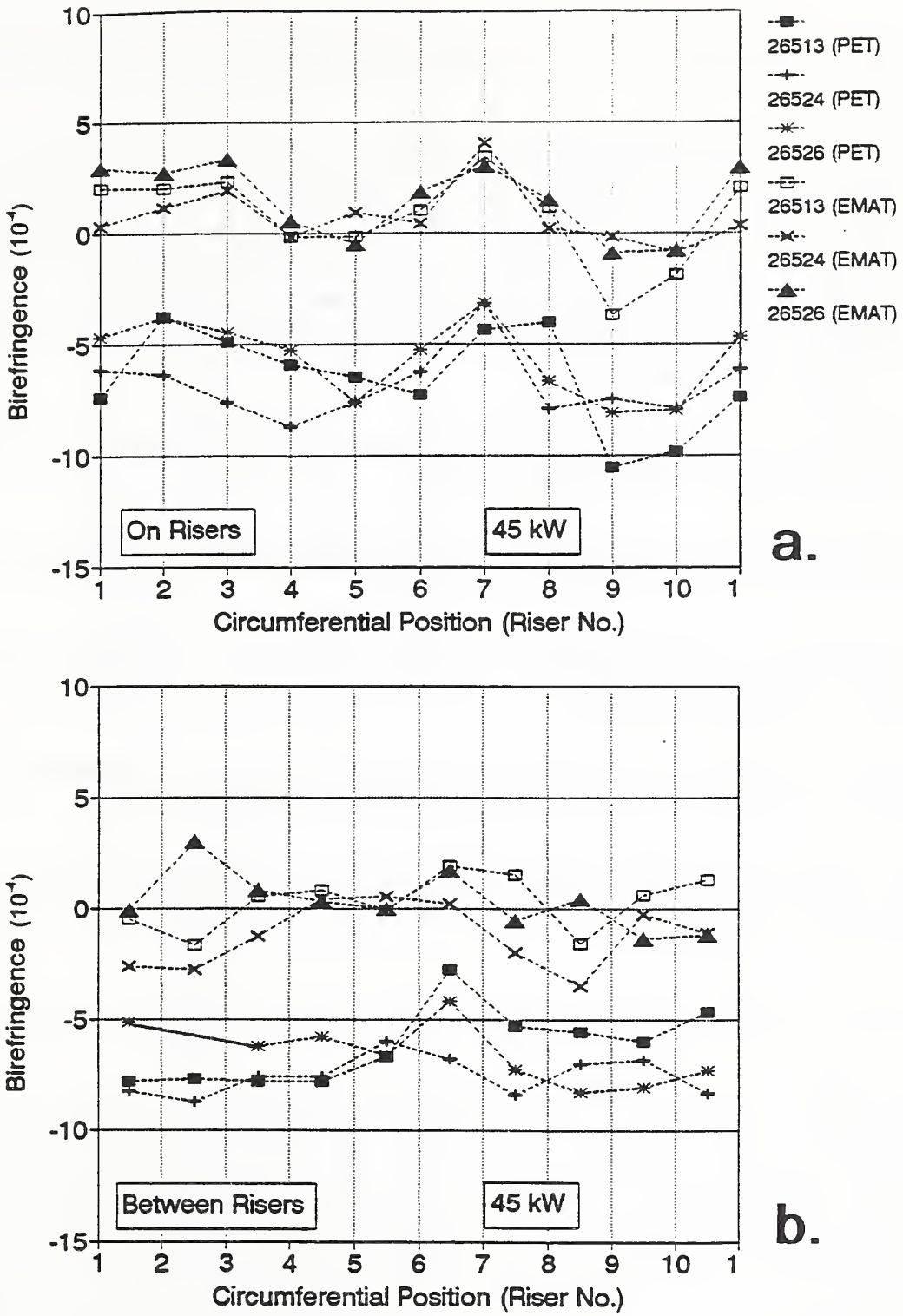

Fig. 16. Birefringence measured with EMAT and PET on 45-kW wheels. a. On risers. b. Between risers.

about 2×10^{-4} in birefringence. This is considerably smaller than the difference in PET and EMAT measurements made at 14 mm and 12 mm, respectively, from the inner rim edge.

To this point all comparisons have been for birefringence. However, the stress predicted by the various birefringence measurements is the point of interest. To convert from birefringence to stress, we used values of B_0 in Table 1. Figure 17 shows the thickness-averaged stresses for our 10 wheels. Here the EMAT brf-repeat data are from the same radial location as the PET data and are in better agreement with them. The trend, as expected, is for hoop stress to increase with the heating power. Again, whenever structure (e.g., local minima in stress) appears in one data set, it appears in all data sets.

Figure 18 summarizes all the birefringence data. Here we averaged the data (for each wheel) at all 20 circumferential locations. The trends are:

1. Stresses from PET measurements are always less compressive (or more tensile) than stresses from EMAT measurements.

2. Stresses from EMAT brf measurements are about 30-MPa more compressive than PET values at the same radial location.

3. Stresses from EMAT measurements (taken 2-mm closer to inner edge of the rim face than PET measurements) were about 50-MPa more compressive than PET values.

4. As the heating increases, all measurements suggest that the thickness-averaged stress becomes more tensile. The stress reverses (becomes zero) at about 42-kW heat input according to PET data.

5. The PET and EMAT data, measured at the same radial location, showed the same trends.

Table 5 summarizes the average stresses from all the measurements. The expected stress level was −140 MPa (−20 ksi) for as-manufactured wheels [22]. The anticipated stress was zero at about 38-kW and significantly tensile at 45-kW [24]. However, finite-element modeling of residual stress buildup due to drag-braking at various powers [26] showed that for brakes centered on-tread, 45-kW heating for 30 min generated a stress of about 35 MPa (5 ksi). If 30-min induction heating (with a coil centered on-tread) is equivalent to this, we conclude that the stresses expected for our 45-kW wheels will be the same, and expect that the maximum thickness-averaged stress will be about 35 MPa. This agrees with data taken with PETs (Table 5).

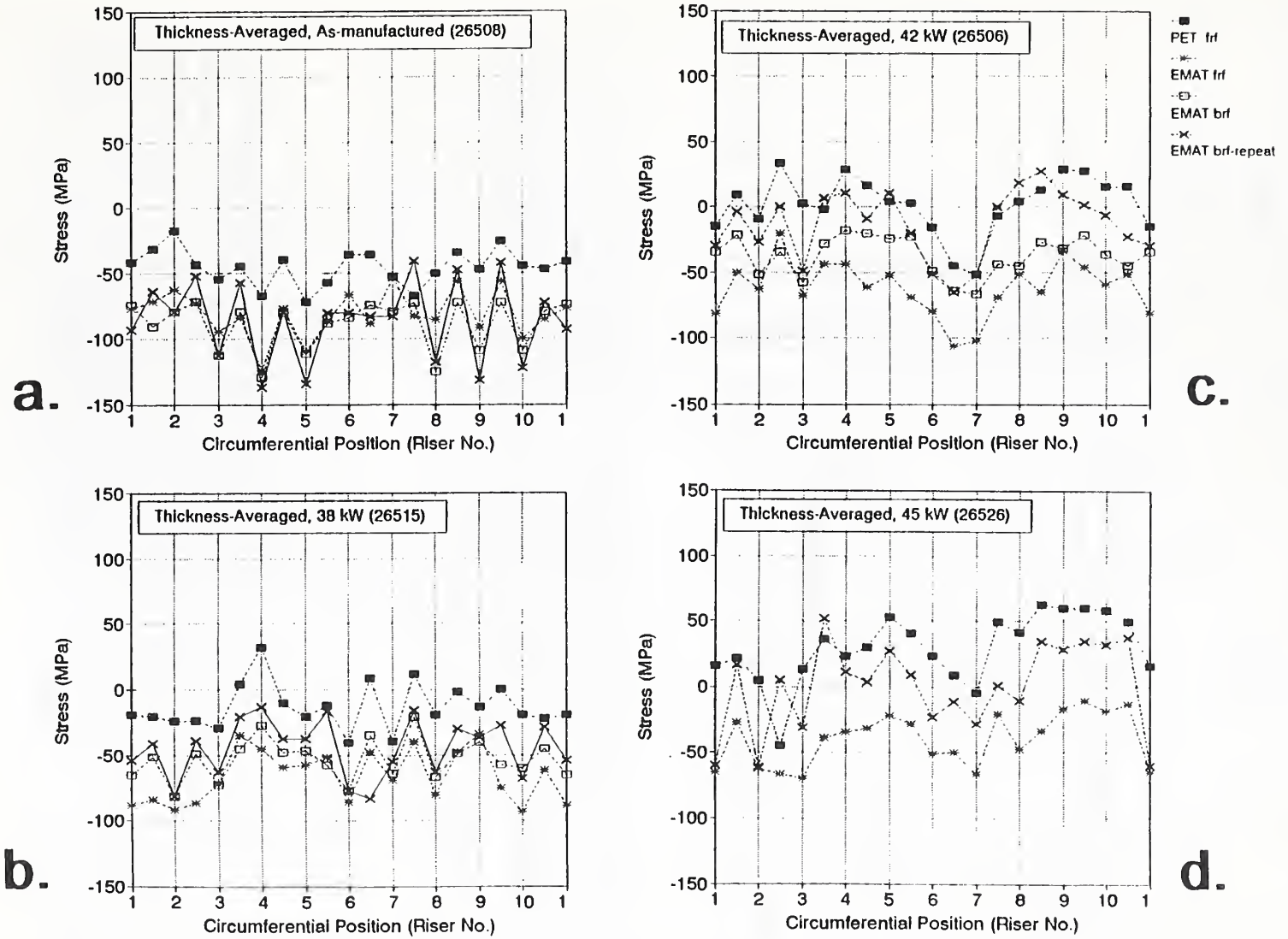

Fig. 17. Through-thickness stress values calculated from birefringences measured by a PET (frf) and an EMAT (frf and brf). a. As-manufactured. b. 38 kW. c. 42 kW. d. 45 kW.

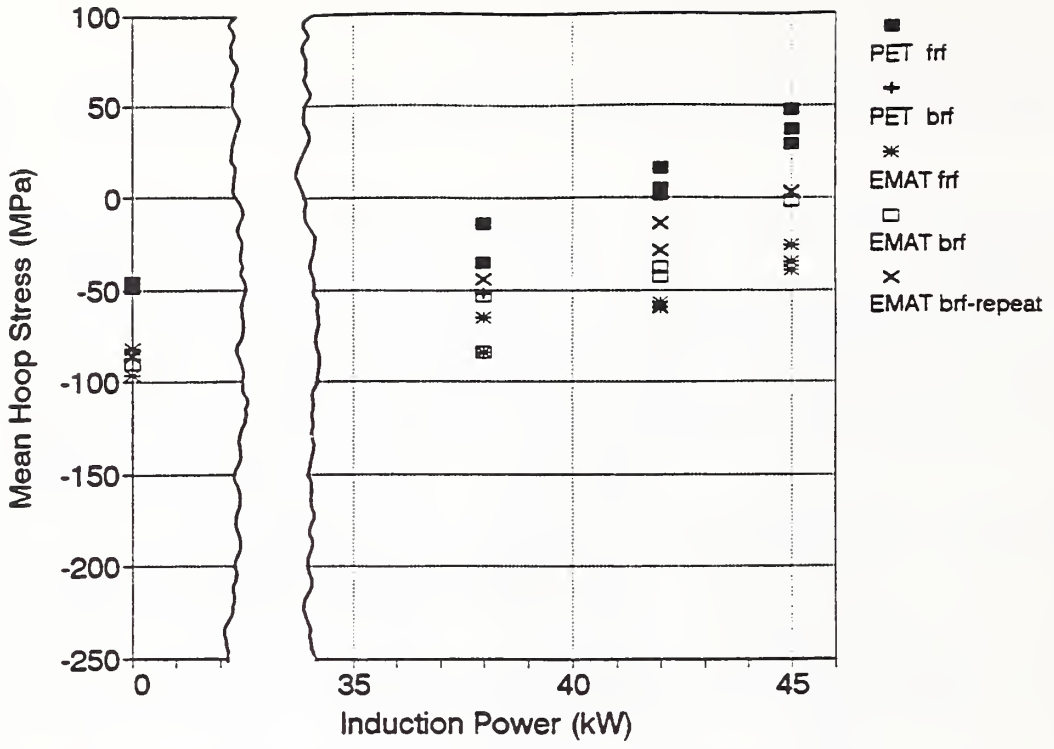

Fig. 18. Summary of through-thickness stress from EMAT and PET birefringence measurements (Fig. 17).

The possibility exists that heat damage could produce out-of-plane bending that would generate tension on one side of the wheel, compression on the other, and a stress gradient through the thickness. This might mean a discrepancy between expected bulk stress and measured stress. If this is the case, surface stress measurements should show different stresses for front and back rim faces. To test this hypothesis, we used the SSW PET probe head to measure TOFs and stresses on both rim faces.

7.3 Surface Stresses Measured on Rim Faces with SSW PETs

The front rim face, even in a new wheel, is narrow and allows only one radial position for the SSW probe head, about 15 mm from the inner rim edge and the center of the acoustic path. Outside this one location, beam spread can cause small spurious echoes from the edge of the rim that interfere with the direct signal and degrade TOF resolution. To convert TOF measurements to stress, we used data from the calibration specimen 46726 from TTC. We assumed that the texture in this multi-wear specimen is the same, as a function of radial position, as in the Griffin test wheels.

Table 5. Summary of through-thickness average stresses calculated from birefringence.

Wheel ID	Thermal power at tread kW (hp)	Average stress MPa (ksi)				
		PET frf	PET brf	EMAT frf	EMAT brf	EMAT brf-repeat
26508	0	-46 (-7)		-82 (-12)	-90 (-13)	-86 (-12)
26512	0	-49 (-7)		-96 (-14)		
26515	38 (51)	-13 (-2)		-65 (-9)	-53 (-8)	-44 (-6)
26524	38 (51)	-35 (-5)	-52 (-8)	-84 (-12)	-88 (-13)	
26506	42 (56)	+2 (0)		-60 (-9)	-37 (-5)	-13 (-2)
26524	42 (56)	+5 (+1)		-59 (-9)	-43 (-6)	-28 (-4)*
26522	42 (56)	+16 (+2)		-57 (-8)		
26513	45 (60)	+37 (+5)		-34 (-5)		
26524	45 (60)	+48 (+7)		-25 (-3)	-1 (0)	
26526	45 (60)	+34 (+5)		-39 (-6)		+3 (0)

*average of 12 points

The surface stresses in Fig. 19 were on the frf. Stresses for wheels with the same heat damage are approximately equal (Table 6). The average stress on the frf becomes more compressive as the heating increases.

The surface stresses in Fig. 20 were on the brf. Since the back faces are wider than the front, two radial positions of the probe were possible. Here r = 15 mm and r = 35 mm are two distances between probe center and inner rim edge. Figures 20a and b show that, for practical purposes, the stresses are the same for both. Therefore, for simplicity in presenting data taken on wheels heated with 42- and 45-kW power, the back face surface stresses shown are mean values for two radial positions. The average brf surface stress values became increasingly tensile with heat. Since the frf data showed the opposite trend (increasing compression), the wheels appear to develop out-of-plane bending (combined compression and tension on opposite

Table 6. Summary of Surface Stresses.

Thermal power at tread (kW)	Wheel ID	Average stress (MPa)	
		frf	brf
0	26508	-137	-96
	26512	-126	-80
38	26515	-165	+7
	26524	-165	-1
42	26506	-186	+44
	26520	-183	+36
	26522	-171	+46
45	26513	-195	+88
	26524	-202	+80
	26526	-209	+94

faces) when heated. As with the through-thickness stresses, the back face surface stresses are not axisymetric, especially for the 42 and 45-kW heated wheels.

We measured the width of heat discoloration on the back side of the plate on several wheels. This band was the result of temperature distribution on the wheel surface during inductive heating. It showed the same circumferential variation as the brf surface stress. (The measure of this band was the distance from the rim edge to a line between red and blue colors.) Figure 21 compares the circumferential distributions of back face surface stress and discoloration for four wheels. The strong correlation shows that variations in SSW TOF measurements are the result of slightly nonaxisymmetric stress distributions.

The additional space available on the back face made it possible to look for any radial gradients in the surface stress by moving the probe head in 5-mm increments from r = 5 mm to 25 mm. The stresses on and between risers are in Fig. 22. There is little stress gradient for both as-manufactured and induction-heated wheels. Again, the surface stress becomes

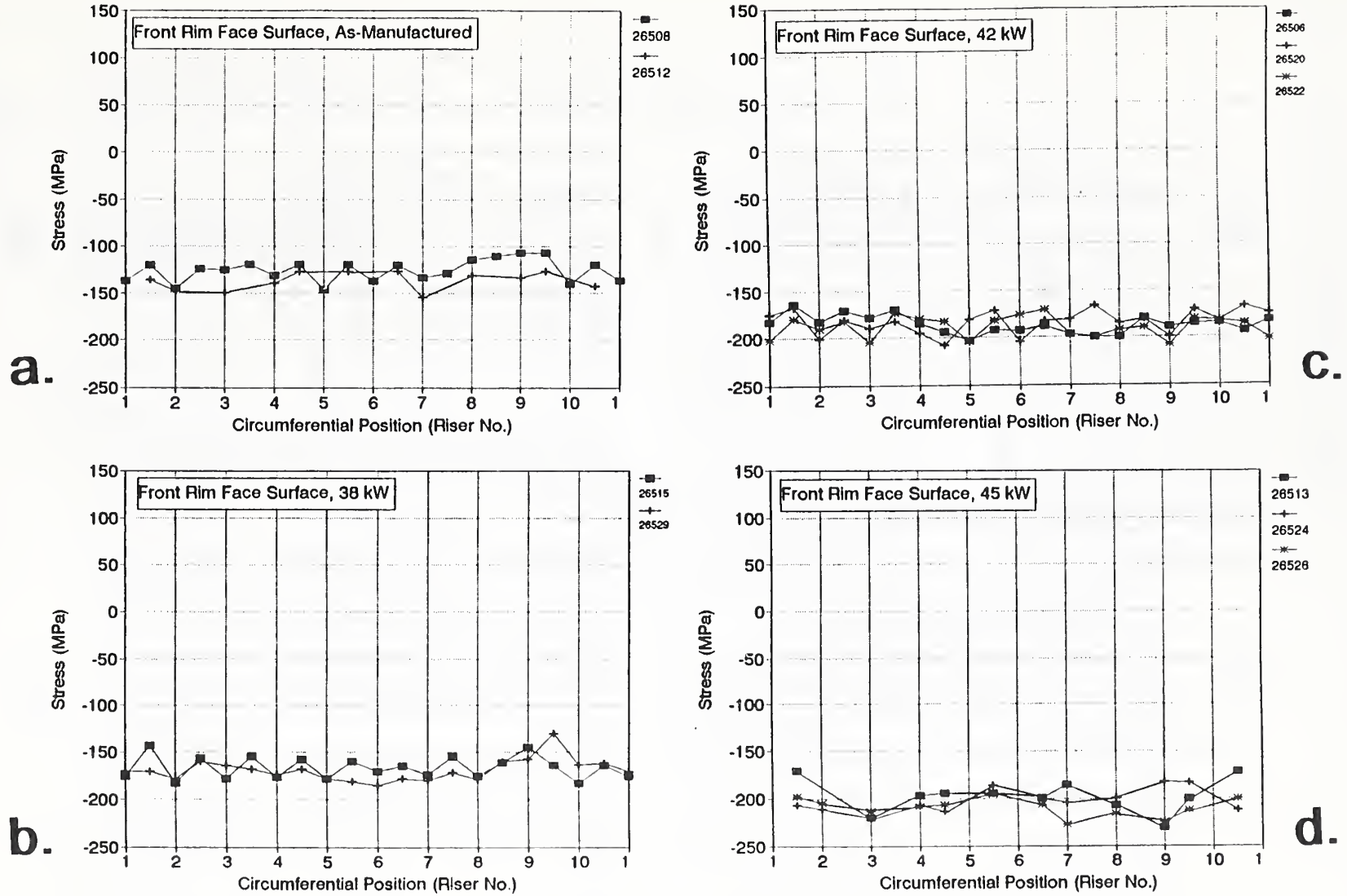

Fig. 19. Surface stresses determined from PET SSW measurements on the frf.
a. As-manufactured. b. 38 kW. c. 42 kW. d. 45 kW.

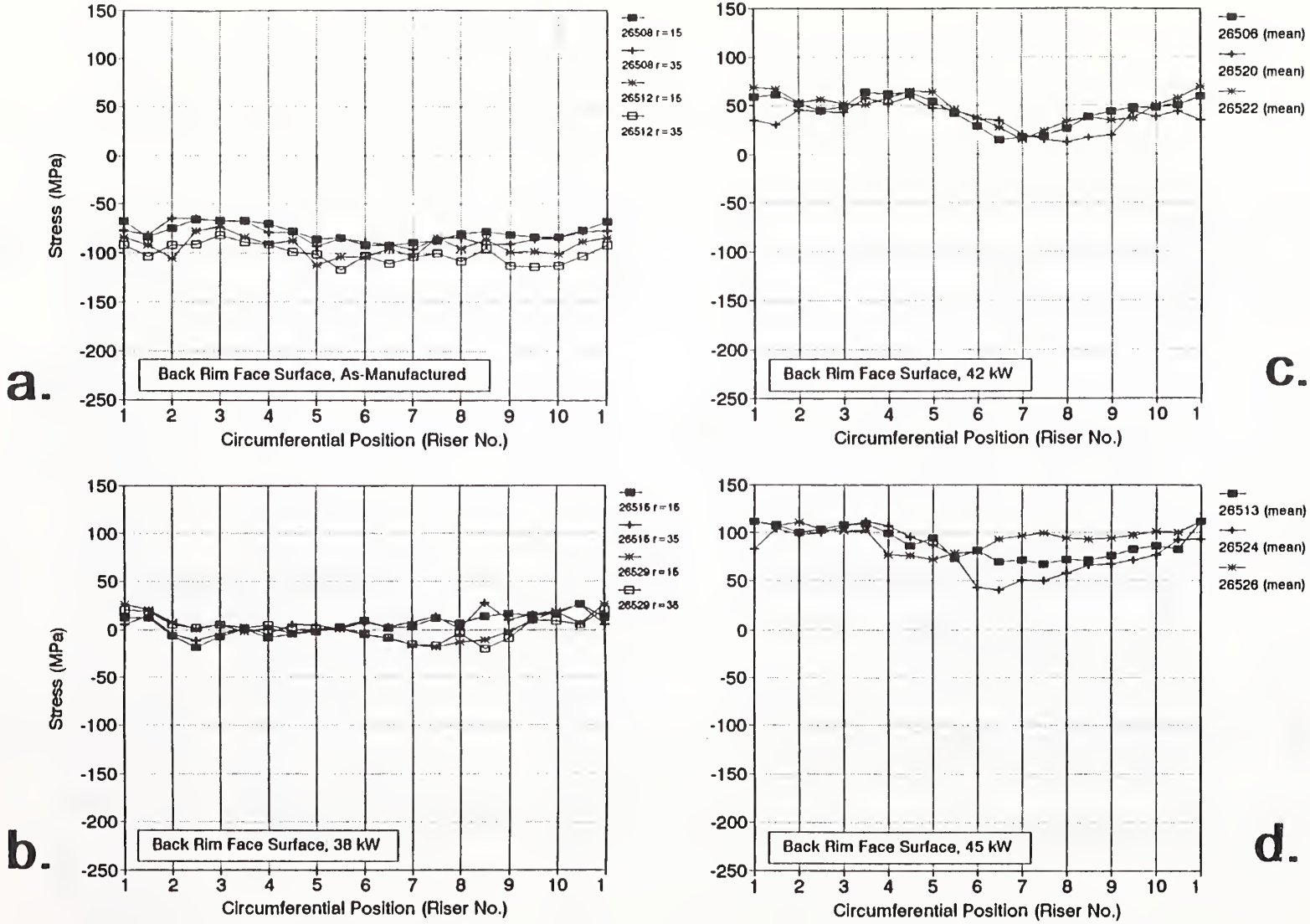

Fig. 20. Surface stresses determined from PET SSW measurements on the brf.
a. As-manufactured. b. 38 kW. c.42 kW. d. 45 kW.

increasingly tensile with heating. Also, there is little difference in radial gradient relative to the risers, probably due to the long gage length.

7.4 Summary of Ultrasonic Measurements

Figure 23 combines the data of Tables 5 and 6 to show mean values of stresses measured with SSWs and birefringence for each group of wheels. As-manufactured wheels show compression on both rim faces and through the rim thickness. For induction-heated wheels, the brf and through-thickness stresses become increasingly tensile with heating; on the frf the state of compression increases. Induction heating introduces not only tension but also a bending component.

Average bulk stress measured with birefringence on as-manufactured wheels is somewhat smaller than the calculated stress [22]. (However, the wheels analyzed in Ref. [22] are about 1000 mm in diameter; the wheels used in our measurements were about 900 mm in diameter). The change between as-manufactured and 45-kW wheels as measured with both PET and EMAT at the same radial location is about 85 MPa. The predicted change in average stress at a location 2-mm further from the tread was 55 MPa, according to EMAT measurements there. Note that, if the wheels are truly in a state of combined bending and tension, the thickness-averaged stress (measured with birefringence) will be lower than the peak stress in the wheels.

All the ultrasonic measurements point to somewhat nonaxisymmetric stresses induced by the induction heating. The discolored band in the wheel plate confirmed this since it showed that heat had not diffused as far into the wheel at low-stress locations.

7.5 Correlation of Ultrasonic and Destructive Measurements

Several of these test wheels will undergo destructive tests using extensive instrumentation to record strains and/or displacements during cutting. From these data, it is possible, in principle, to calculate residual stresses.

A simpler alternative is the incremental damage curve [27]. After induction-heating to various levels, several wheels were cut along a radius with a saw starting at the flange tip. Depending on the direction and degree of stress in the rim, the tip opened or closed as the blade penetrated. A plot of this displacement D as a function of the saw cut depth at the different powers is the incremental damage curve and gives a measure of the overall stress state in the wheel.

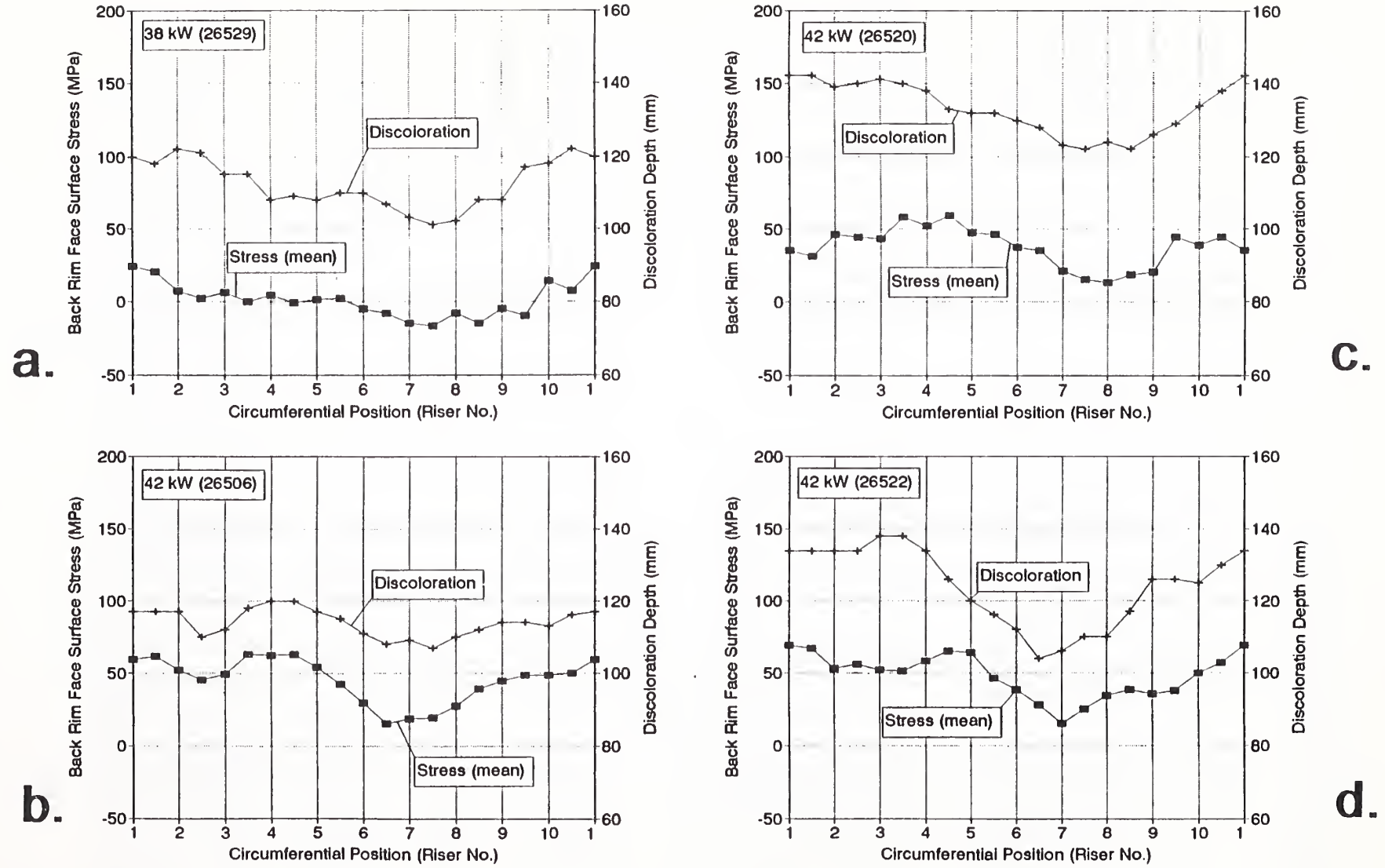

Fig. 21. Comparison of surface stress and depth of discoloration due to heating.
a. 38 kW (26529). b. 42 kW (26506). c. 42 kW (26520). d. 42 kW (26522).

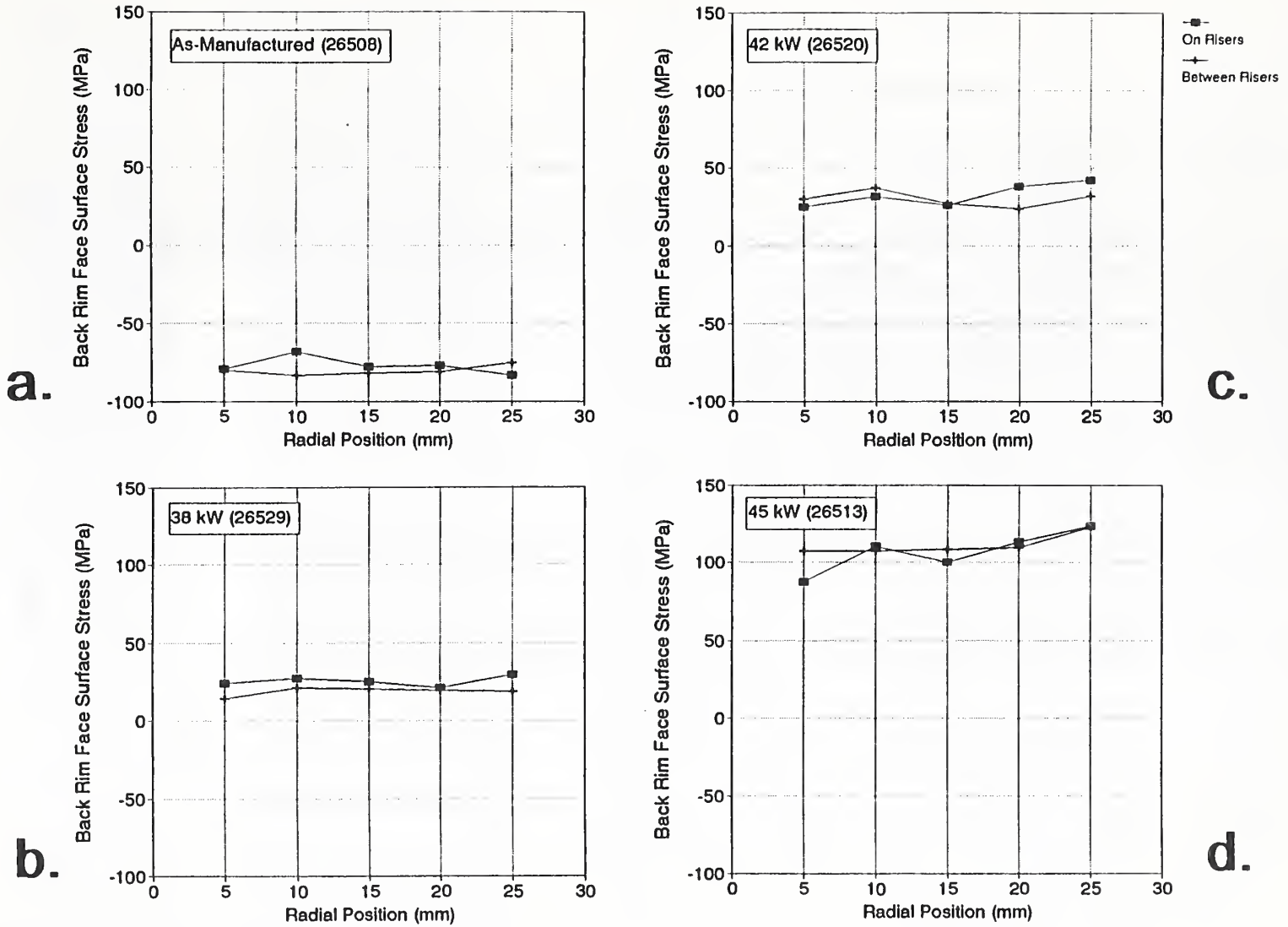

Fig. 22. Radial variation of surface stress on brf.
a. As-manufactured (26508). b. 38 kW (26529). c. 42 kW (26520). d. 45 kW (26513).

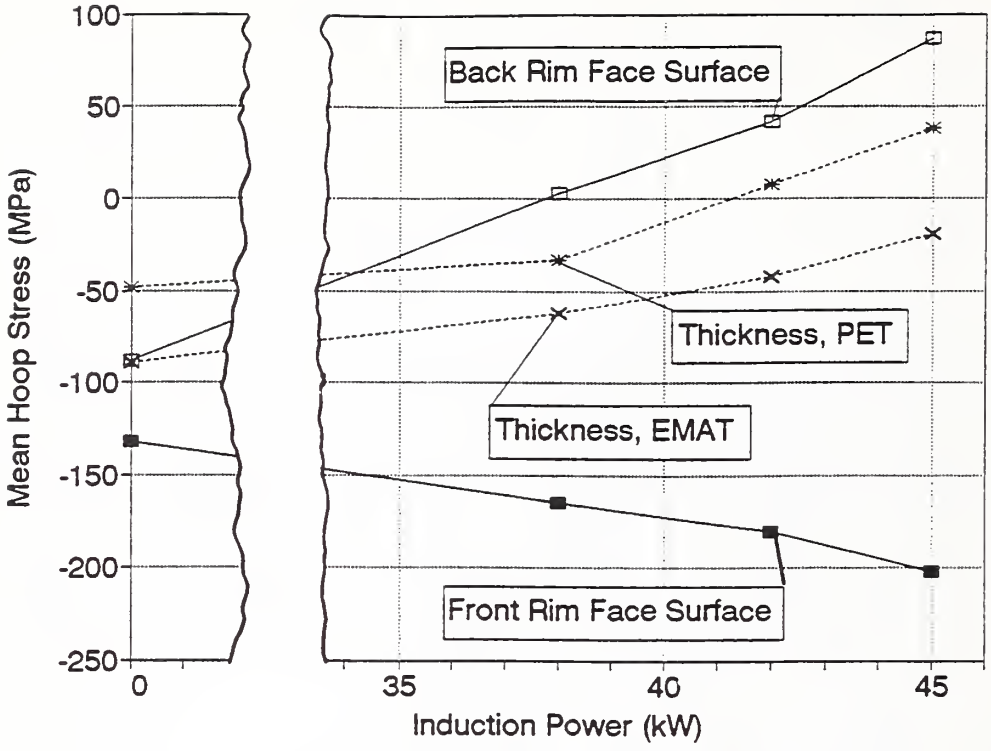

Fig. 23. Composite of surface and thickness-averaged stresses. These results suggest a state of combined bending and tension for induction-heated wheels.

The Appendix shows that saw cut opening is an indicator of the net rim force F_N when the saw cut extends through the rim area. This may be a convenient measure of wheel safety. Typically failure occurs when fatigue cracks, originating on the wheel surface, extend into a region of tensile stress. If the cracks encounter a region of compression, crack arrest is likely. F_N is the integral of σ_θ over the rim area. If $F_N > 0$, then it is likely that a crack will encounter a tensile area and grow. If $F_N < 0$, crack arrest is more likely. In this light, we seek a correlation of our ultrasonic measurements with F_N, which is related to the saw cut opening D when the cut extends through the rim.

To this end, three induction-heated wheels went back to the manufacturer for saw cutting: 26529 (38 kW), 26520 (42 kW), and 26513 (45 kW). The ultrasonic data indicated a minimum of stress around location 7 (Fig. 20), so all three wheels were cut there. To obtain additional data, there were also cuts at location 2, 180° around the rim (Fig. 4). For saw cuts extending only through the rim area, there should be minimal stress relief on the opposite side of the wheel [24].

The results of the saw cutting for the three induction-heated wheels are in Table 7 [24]. The saw cut opening cited corresponded to a depth of 76 mm (3 in), completely stress-relieving the rim area. For comparison, we also include a saw cut opening for an as-manufactured wheel from a different production run [27]. Due to the tightly controlled production procedures, we expect a similar result for as-manufactured wheels in our test set.

The data clearly show that less opening occurred at location 7 than at location 2, as expected from the ultrasonic data. Figure 24 shows the saw cut data as a function of: back face surface stress, PET birefringence at 14 mm from the inner rim edge, and EMAT birefringence at 12 mm from the inner rim edge. In this figure, we have averaged the birefringence data(made with a typical aperture of about 10 mm × 10 mm) to suppress scatter and allow a more valid comparison with surface stress data (made over a path length of 200 mm). For the PET birefringence data, we averaged data from locations 1, 2, and 3, and from locations 6, 7, and 8. For the EMAT birefringence data we averaged the measurements at locations 1.5 and 2.5, and at locations 6.5 and 7.5.

Clearly, there is a very good correlation between surface stress measurements on the brf and the saw cut displacement D. The next best correlation is between the birefringence data (bulk stress) at 14 mm from the inner rim edges. The correlation was not quite as good for birefringence measurements at 12 mm (2 mm farther from tread area). The good correlation with surface stress is not unexpected, since Fig. 23 shows that induction heating causes the largest change in brf surface stresses. The apparent state of combined bending and tension causes the bulk stresses to increase more slowly with heating.

While it is useful to compare absolute stresses (as measured with ultrasonics) with destructive measurements, it is probably more important to distinguish wheels in tension ($F_N > 0$) from those in compression ($F_N < 0$). Thus, there may be no particular advantage to using a set of rimblocks to obtain B_0 for absolute stress determination. Since we found that the off-riser birefringence was uniform for our as-manufactured wheels, we could as well measure relative changes in stress between induction-heated and as-manufactured wheels. Furthermore, the simplest stress measurement method is preferable, and this appears to be the measurement of birefringence on the frf.

Pursuing this, we calculated from the PET frf birefringence data: (1) The average stress for both as-manufactured wheels from Table 5 (-48 MPa). (2) The average saw cut opening displacement for each heating level from the data in Table 7. (In effect, we assume more scatter in the ultrasonic results than in the saw cutting.) Figure 25 shows the change $\Delta\sigma$ in average stress with the average saw cut opening. The data show that 9 of the 10 wheels would be

Table 7. Saw cut opening displacement for selected wheels.

Wheel ID (power, kW)	Location (riser)	Opening (μm)
---* (0)	---	-287
26529 (38)	2	89
	7	20
26520 (42)	2	280
	7	220
26513 (45)	2	440
	7	330

* This wheel was not from the current test set [27].

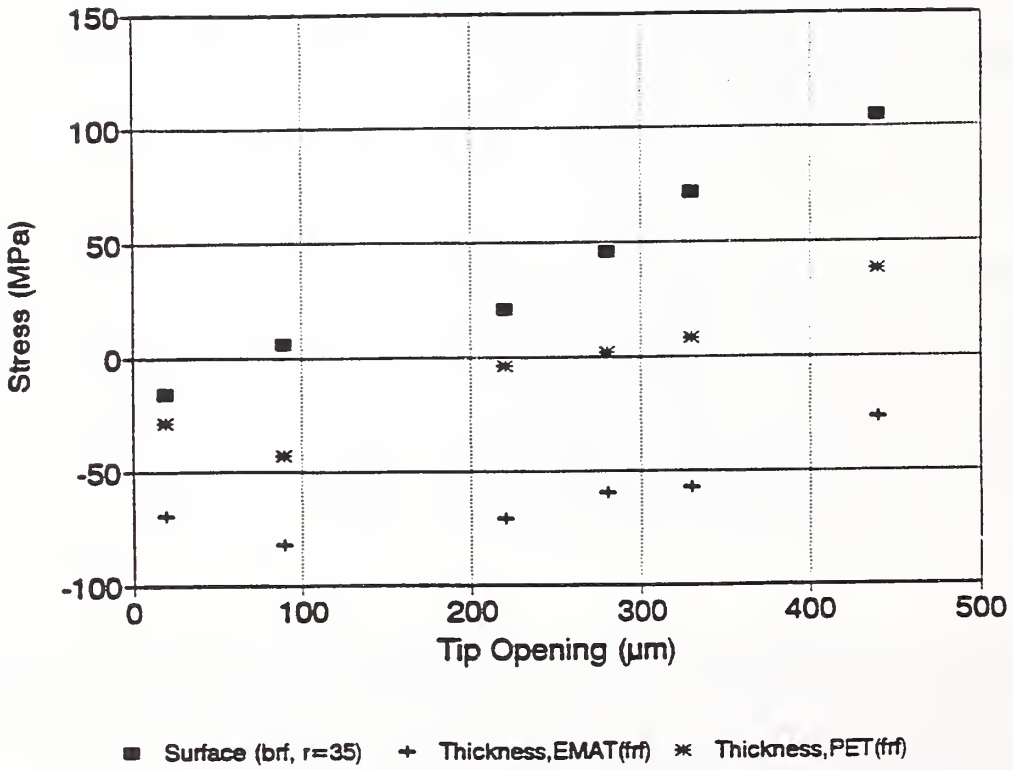

Fig. 24. Comparison of absolute stress values (determined from ultrasonics) with saw cut-opening displacement D after a 76-mm deep cut.

properly classified as either tensile or compressive. The sole exception is one outlier (a 38-kW wheel) that would be improperly classified as compressive.

A simple measure of overall stress state, such as D, is useful since a detailed analysis of saw cut wheels is laborious and time-consuming. Also, it is likely that in-service wheels will have more complicated stress distributions than our induction-heated wheels. Indeed, they may have a wide range of stress distributions, so extrapolating from the detailed DE of induction-heated wheels to in-service wheels may not be possible. However, it will be relatively simple to saw cut many in-service wheels to obtain a large data base on a simple measure of damage, such as D.

8. CONCLUSIONS

To test ultrasonic NDE for application to the measurement of residual stress in railroad wheels, we have made over 1,000 stress measurements on a set of 10 unused wheels. Two were as-manufactured and eight were induction-heated to generate three levels of damage. This method of specimen preparation was faster and less expensive than drag-braking; also, the assumption was that induction heating would induce more axisymmetric stress and simplify the destructive tests to validate the ultrasonic measurements.

The NDE used two distinct types of ultrasonic transducers. The EMAT system, developed at NIST, generates and receives shear waves propagating through the rim thickness. The EMAT has the advantage of not requiring any acoustic couplant between transducer and specimen (in contrast to piezoelectric transducers). Scanning to obtain data at different circumferential locations is easy and will be important if stresses are not axisymmetric. However, the EMAT has multiple transduction mechanisms on magnetic materials that can generate waves interfering with each other and degrading the TOF (and stress) resolution. In our case, the Lorentz force mechanism was expected to dominate the magnetostriction mechanism, allowing good resolution.

To test this hypothesis, we also employed a PET system. Magnetic artifacts do not affect piezoelectric transduction, so this system serves as a benchmark against which to compare the EMAT system. The PET was insensitive to the degree of surface preparation. Also, measurements made from both frf and brf were in good agreement, indicating that beam spread (and hence reflection from the tread) were insignificant in their influence on TOF resolution. Furthermore, measurements made with PETs having different apertures were also in good agreement, another sign that beam spread in the rim is negligible. In essence, the difference between ultrasonic system results is less significant (leads to less uncertainty) than

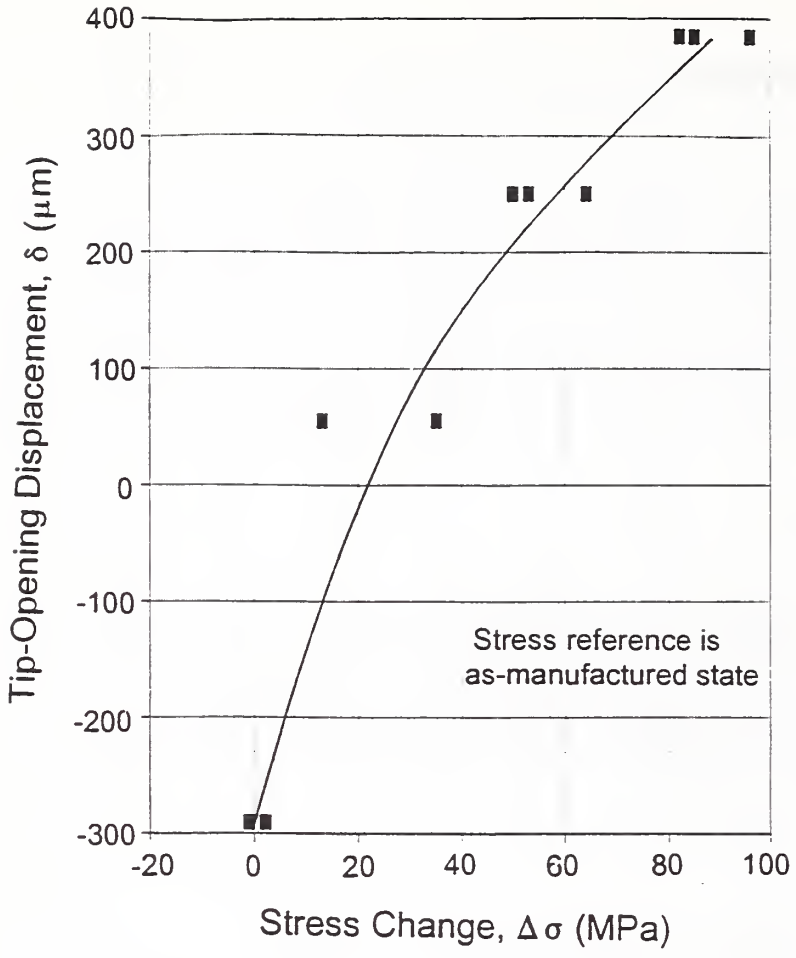

Fig. 25. Comparison of changes in stress from as-manufactured state (as measured with birefringence) with saw cut-opening displacement D.

the scatter in B_0 values. This scatter (SD in equivalent stress uncertainty of ±50 MPa) is presumably from slight variations in the texture of the cast product.

Ten stress-relieved rimblocks were the baseline references for birefringence due to texture. PET and EMAT measurements in the center of the frf showed good agreement in that the average value of B_0 (the unstressed birefringence) was almost the same for both systems (to within parts in 10^4). Because of material variability, B_0 was different for each rimblock. Calculating SD/C_A gave ±50 MPa as a measure of stress resolution when using the entire rimblock population to remove the influence of texture. Previous measurements [15] had shown that the SD might be smaller in rimblock populations from individual plants. Since all of the test wheels were from one plant, we used the subset of rimblocks from that plant for B_0 (Table 1).

Birefringence measurements with both PET and EMATs were made at a radial location of 14 mm from the inner edge of the frf. Additional EMAT sets were at 12 mm from frf and brf. Comparison shows that the two systems, at the same radial location, agreed within about 30 MPa (4 ksi), on the average; as a practical matter, this is excellent agreement.

The bulk stresses became more tensile with heat damage, as expected. Stress reversal, predicted from PET measurements, occurred at about 42 kW (56 hp), slightly higher than the 38 kW (51 hp) seen in saw cutting [27] and Table 7. At 45 kW (60 hp), the PET values reached a maximum of about 35 MPa (5 ksi), somewhat less than expected [24]. However, finite element calculations [26] had predicted an average (bulk) stress of about 35 MPa for this power, agreeing with the PET results.

The lower than expected bulk stresses may be due to the presence of a bending component. As thermal damage increased, the SSW PET device found that surface stresses on the brf became more tensile, changing from about -90 MPa (as-manufactured) to about +90 MPa (45 kW). The bulk stress measurements follow this trend, but are lower, on average. In contrast, the surface stresses on the frf became increasingly compressive, although the change was considerably smaller, from -135 MPa (as-manufactured) to about -200 MPa (45-kW).

In the as-manufactured condition, the stress is uniform through the rim thickness. (Figure 23 shows bulk and surface stresses to be almost the same.) As the heating power increases, a gradient develops through the thickness. The stresses change more rapidly near the brf, going from compressive to tensile. In the remainder of the rim thickness, the stress is more uniform. This would explain why bulk stresses are closer to brf stresses for heated wheels.

The ultrasonic NDE and the visual plate discoloration exhibited a slightly non-axisymmetric stress in the heated wheels. DE by saw cutting three damaged wheels along radii at risers 2 and 7 confirmed a smaller stress at the latter location.

As a practical matter, it may not be critical that ultrasonic measurements of stress agree exactly with destructive measurements. What may be more important is to correlate a measure of stress (e.g., bulk stress) with some simple destructive test, such as saw cutting. Since in-service residual stress distribution can be complex, a simple measure of the general stress state (such as saw cutting) may be more practical for rapid assessment of possible wheel damage. This idea is the basis of the incremental damage curve approach [27].

The displacement of the flange tip opening during saw cutting correlated well with both surface and bulk stress for our test wheels. The best correlation was for the brf surface stress, in part because it increases more rapidly with heating than bulk stress. The next best correlation was

with bulk stress measured at 14 mm from the inner rim edge (near the center of the rim face), while the link with bulk stress at 12 mm (2 mm farther from tread) was not quite as good.

For wheel shop implementation, the most practical NDE approach probably will be the use of EMATs to check bulk stress. In fact, the Deutsches Bundesbahn currently has such a system under evaluation for wrought wheels of European manufacture [28]. It appears that bulk stress measured at the center of the rim face should be able to distinguish wheels in compression from those in tension. If the correlation holds for in-service wheels, it should be possible to discriminate between safe and unsafe wheels in a timely and reliable manner.

In summary:

1. We made over one thousand measurements of bulk and surface residual stress, using both PET and EMAT ultrasonic systems.

2. Bulk stresses measured with PET and EMAT at the same radial locations came to within 30 MPa (4 ksi) of each other, on the average. This is good agreement for residual stress measurement using different sets of instrumentation.

3. The trend was increasingly tensile bulk stress as heating power increased.

4. Surface stress on the back face displayed the same trend. The stress change from as-manufactured to the 45-kW wheels was about +180 MPa.

5. Surface stress on the front face showed the opposite trend. The stress change from as-manufactured to the 45-kW wheels was about -65 MPa.

6. These results (3, 4, and 5) imply a gradient of stresses through the rim thickness, with the gradient steeper near the frf. In effect there is combined out-of-plane bending and hoop tension in the severely heated wheels.

7. The flange tip displacement during radial saw cuts closely followed the ultrasonic NDE.

ACKNOWLEDGMENTS

We are indebted to the Federal Railroad Administration for funding this research, and to our contract monitor, Donald Gray, for considerable guidance. The Association of American Railroads in Chicago and their Transportation Technology Center in Pueblo, Colorado, have

provided us with information, insights, and rimblock specimens; we are particularly grateful to Robert Florom and Dan Stone. Griffin Wheel Co. and Michael Gallagher were invaluable in providing our test wheels, induction heating them, and supplying their prior data. Julian Deputat of the Institute of Fundamental Technological Research of the Polish Academy of Sciences made possible both the visit of Jacek Szelążek to our laboratory and the use of the DEBRO instrument.

9. REFERENCES

1. J.H. Armstrong, "Keeping Wheels in Shape," Railway Age, Feb. 1985, pp. 39-48.

2. Federal Railroad Administration, U.S. Dept. of Transportation, Code of Federal Regulations 49 CFR, 65, §215.03(h), 1985.

3. Office of Research and Development of the Association of American Railroads, *Wheel Failure Mechanisms of Railroad Cars*, Report TFR 53-82-C-00282, 1986.

4. J.R. Barton, W.D. Perry, R.K. Swanson, G.C. Hsu, and S.R. Ditmeyer, "Heat-Discolored Wheels: Safe to Reuse?" Progressive Railroading, Mar. 1985, pp. 41-48.

5. K.-O. Edel, H. Hintze, and M. Korn, "Analysis of a Solid Railway Wheel Breakage," *Rail International*, Jan., 1992, pp. 28-40.

6. Y.-H. Pao, W. Sachse, and H. Fukuoka, "Acoustoelasticity and Ultrasonic Measurements of Residual Stresses," *Physical Acoustics*, Vol. XVII, W.P. Mason and R.N. Thurston, eds. (Academic Press, NY, 1984), pp. 61-143.

7. K. Okada, "Stress-Acoustic Relations for Stress Measurement by Ultrasonic Technique," Journal of the Acoustical Society of Japan (E) 1(3): 193-200, 1980.

8. H. Fukuoka, H. Toda, K. Hirakawa, H. Sakamoto, and Y. Toya, "Acoustoelastic Measurements of Residual Stresses in the Rim of Railroad Wheels," *Wave Propagation in Inhomogeneous Media and Ultrasonic Nondestructive Evaluation*, Vol. 6, ed., G. C. Johnson (ASME, NY, 1984), pp. 185-193.

9. A.V. Clark, Jr., H. Fukuoka, D.V. Mitraković, and J.C. Moulder, "Characterization of Residual Stress and Texture in Cast Steel Railroad Wheels," Ultrasonics 24: 281-288, 1986.

10. *Draft Control Committee Office for Research and Experiments of the International Union of Railways*, Question B169, Effect of Frequent Braking on Residual Stress Field in the Wheel Rim, Utrecht, The Netherlands, Report No. 2, April 1989.

11. J. Deputat, A. Kwaszczyńska-Klimek, J. Szelążek, "Monitoring of Residual Stresses in Railroad Wheels with Ultrasound," *Proceedings of the Twelfth World Conference on Nondestructive Testing*, Amsterdam, The Netherlands, Paper No. 191, 1989.

12. J. Deputat, "Effect of Braking Application on Residual Stress in the Rim of Railroad Wheels," *Proceedings of the Conference on Rolling Noise Generation*, Technische Universität, Berlin, Germany, September 1989, pp. 159-168.

13. H.C. Iwand, "A Comparative Analysis Using Barkhausen Noise Analysis Ultrasonic Birefringence, and Saw Cutting Techniques in Determination of Residual Stress in Railroad Wheels," Thesis, University of Nebraska, Lincoln, 1988.

14. R.B. Thompson, "Physical Principles of Measurements with EMAT Transducers," *Physical Acoustics*, Vol. XIX, R.N. Thurston and A.D. Pierce, eds. (Academic Press, NY, 1990), pp. 157-200.

15. R.E. Schramm, A.V. Clark, Jr., D.V. Mitraković, S.R. Schaps, and T.J. McGuire, "Report No. 23 - Residual Stress Detection in Railroad Wheels: An Ultrasonic System Using EMATs," NISTIR 3968, National Institute of Standards and Technology, 1991.

16. R. E. Schramm, A. V. Clark, and T. J. McGuire, "Ultrasonic Measurement of Residual Stress in Railroad Wheel Rims," *Proceedings, Tenth International Wheelset Congress*, National Conference Publication (The Institution of Engineers, Australia, Sydney, 1992), pp. 151-155.

17. A. Wilbrand, "Quantitative Modeling and Experimental Analysis of the Physical Properties of Electromagnetic-Acoustic Transducers," *Review of Progress in Quantitative Nondestructive Evaluation*, Vol. 7A, D. O. Thompson and D. E. Chimenti, eds. (Plenum Press, NY, 1988), pp. 671-680.

18. R.B. Thompson," A Model for the Electromagnetic Generation of Ultrasonic Guided Waves in Ferromagnetic Metal Polycrystals," IEEE Transactions on Sonics and Ultrasonics SU-25(1), 1978, pp. 7-15.

19. A. Brokowski and J. Deputat, "Ultrasonic Measurements of Residual Stress in Rails," *Proceedings, Eleventh World Conference on Nondestructive Testing*, Vol. 1 (The World Conference on Nondestructive Testing, Columbus, OH, 1985), pp. 592-598.

20. A. Brokowski and J. Deputat, "Ultrasonic Investigations of the Influence of the Degree of Deformation on the Distribution of Elastic Properties in Iron," *Proceedings of the Conference on Non-Destructive Testing* (Institute of Fundamental Technological Research, Polish Academy of Sciences, Warsaw, Poland, 1982), pp. 37-42 (in Polish).

21. J. Deputat, "Ultrasonic Technique for Measuring Stresses in Screws," *Proceedings, Ninth World Conference on Nondestructive Testing* (The World Conference on Nondestructive Testing, Columbus, OH, 1979), Report 4 EDD-2.

22. C. Kuhlman, H. Sehitoglu, M. Gallagher, "The Significance of Material Properties on Stress Developed During Quenching of Railroad Wheels," *Proceedings ASME/IEEE Railroad Conference*, V. T. Hawthorne and T. Kneschek, eds. (American Society of Mechanical Engineers, NY, 1988), pp. 55-63.

23. DEBRO Ultrasonic Stress Meter, Institute of Fundamental Technological Research, Polish Academy of Sciences, Warsaw, Poland, 1990.

24. M.T. Gallagher, Griffin Wheel Co., Chicago, IL, private communication.

25. A.V. Clark and Y. Berlinsky, "Effect of Liftoff on Accuracy of Phase Velocity Measurements Made with Electromagnetic Acoustic Transducers," Research in Nondestive Evaluation 4: 79-96,1993.

26. M.T. Gallagher, M.A. Polzin, and C.D. Christie, "Railroad Wheel Flange Failures: Causes and Preventions," RTD-Vol. 5, *Rail Transportation*, Book No. G00767 (ASME, NY, 1992), pp. 155-163.

27. M.T. Gallagher and M.A. Polzin, "Defining the Thermal Tolerance of Curved Plate Heat Treated Wheels," *Proceedings, Tenth International Wheelset Congress*, National Conference Publication (The Institution of Engineers, Australia, Sydney, 1992), pp. 33-38.

28. E. Schneider, R. Herzer, D. Bruche, and H. Frotscher, "Reliability Assurance of Railroad Wheels by Ultrasonic Stress Analysis," *Third European Conference on Residual Stresses*, Nov. 4-6, 1992, Frankfurt, Germany.

29. R.A. Beth, "Statics of Elastic Bodies," *Handbook of Physics*, E.U. Condon and H. Odishaw, eds. (McGraw Hill Book Co., NY, 1958), pp. 3-64.

10. APPENDIX: Calculation of Net Rim Force

In one DE method for rim stresses, a saw blade cuts into a wheel along a radius at hoop position $\bar{x}$. The wheel displacement at the cut (opening or closing) is given by

$$u(\bar{x}) = \int G(\bar{x},\bar{\xi})\sigma_\theta(\bar{\xi})d\bar{\xi}, \qquad \text{(A-1)}$$

where $G(\bar{x},\bar{\xi})$ is the compliance or influence function (Green's function) that gives the displacement at $\bar{x}$ due to the load at $\bar{\xi}$, and $\sigma_\theta(\bar{\xi})$ is the hoop stress at $\bar{\xi}$.

By Saint-Venant's principle [29], if the forces acting on a small portion of an elastic body are replaced by an equivalent system of forces, the redistribution of loads may produce substantial stress changes locally but the effect is negligible at distances large in comparison with the linear dimensions of the region on which the forces are changed. Systems of forces that are statically equivalent have the same resultant force and moment of force. This can easily be demonstrated from eq (A-1). In general, $G(\bar{x},\bar{\xi})$ varies as $|\bar{x}-\bar{\xi}|^{-m}$ away from $\bar{\xi}$ (m>0). Thus, if $\bar{x}$ is at some distance from $\bar{\xi}$, and if σ_θ has a relatively steep gradient, then $G(\bar{x},\bar{\xi})$ can be taken outside the integral (essentially replaced by a constant, K). Then we have $u = KF_N$, where

$$F_N = \int \sigma_\theta(\bar{\xi})d\bar{\xi}; \qquad \text{(A-2)}$$

that is, F_N is the net rim force.

Furthermore:

- If the hoop stresses are compressive, then $F_N < 0$, and rim cracks will probably arrest, so the wheel is safe.

- If the hoop stresses are tensile, then $F_N > 0$, and rim cracks may grow, so the wheel is unsafe.